8-2014

An Evaluation of Void Formation in Ex-Service and Creep Tested HP Alloy Tubing Used for Hydrocarbon Reforming

Zane William Fox Palmer
University of Tennessee - Knoxville, zpalmer@utk.edu

To the Graduate Council:

I am submitting herewith a thesis written by Zane William Fox Palmer entitled "An Evaluation of Void Formation in Ex-Service and Creep Tested HP Alloy Tubing Used for Hydrocarbon Reforming." I have examined the final electronic copy of this thesis for form and content and recommend that it be accepted in partial fulfillment of the requirements for the degree of Master of Science, with a major in Materials Science and Engineering.

Carl D. Lundin, Major Professor

We have read this thesis and recommend its acceptance:

Hahn Choo, Easo P. George

Accepted for the Council:
Carolyn R. Hodges

Vice Provost and Dean of the Graduate School

(Original signatures are on file with official student records.)

An Evaluation of Void Formation in Ex-Service and Creep Tested HP Alloy Tubing Used for Hydrocarbon Reforming

A Thesis Presented for the

Master of Science

Degree

The University of Tennessee, Knoxville

Zane William Fox Palmer

August 2014

Abstract

HP alloy tubing is commonly used in petroleum reforming facilities for its high temperature strength and resistance to corrosion. Unfortunately, the tubes can experience failure during service caused by the formation of voids in the tube wall brought on by creep stress generated by the pressure differential and thermal gradient between the inside and outside diameters of the tube. The purpose of this project was to analyze the formation of voids in eight ring sections, each from a different ex-service tube, from a total of three different manufacturers (identified as M1, M2, and M3). Further analysis of the ex-service tubes was done by evaluating eighteen creep tested samples removed from the eight ex-service tubes. For both the service exposed and the creep tested samples, the general location for preferential void formation was identified as being in the fine grain region of the tubes at the inside diameter. Furthermore, it was determined that the tubes from manufacturer M1 are more resistant to damage during service than the tubes from manufacturers M2 and M3. Despite being exposed to the highest service temperature and longest service exposure, the tubes from manufacturer M1 had no indication of damage upon removal from service and experience the lowest amounts of void formation.

Table of Contents

List of Tables

List of Figures

1: Project Description

Petroleum and natural gas refineries are a vital part of the global energy infrastructure, processing raw, unrefined crude oil or natural gas into fuels and useful byproducts. This project specifically focuses on the tubing found in reformer plants that break down natural gas into products like methane, propane and hydrogen. These plants work like large distilleries, applying high temperatures and pressures to force the reaction gas through a catalyst and "boil off" the lighter compounds, allowing the products to separate via weight along the length of the vertical tube.

This project analyzed void formation in eight ex-service HP alloy tubes from five different reforming plants made by three different manufacturers as well as a total of eighteen creep tested samples removed from sections from the eight tubes. The tube ring sections were analyzed for swelling, with samples being removed from the thickest wall section of the ring, the area of least expected damage, for optical characterization. Samples were also removed from each of the rings for chemical analysis. The creep samples, tested to within approximately 95% of life, were obtained for optical light microscopy (OLM) characterization to analyze changes in microstructure and void content resulting from creep. The creep samples were received from MTI (a commercial laboratory in Ann Arbor, MI) and were removed from the parent tubes and tested in the circumferential and longitudinal directions with respect to the tube wall

Optical characterization was performed on the ex-service and well as creep tested samples in order to evaluate their microstructures, grain structure, and void distribution. An analysis of optical light microscope (OLM) images was accomplished to evaluate microstructure and void formation, while macro analysis was performed in order to analyze the orientation and distribution of grains within the tube samples.

2: Literature Review

2.1: Environment

The primary use of HP alloy steel is as reforming furnace reaction tubes used in petroleum refining. These tubes are oriented vertically, and have a feeder gas injected into the bottom of the tube through a solid catalyst. Through the application of high temperatures, typically between 1550 and 1950°F, the catalyst breaks down the feeder gas into hydrogen and/or lighter hydrocarbon chains. The vertical orientation of the tubes acts as a distillation column, with the heavier feeder gas remaining at the bottom of the column with the catalyst and the lighter reaction products traveling up the tube where they are then extracted. Due to the large size of the reaction tubes, compensation systems are used to reduce the stress on the tube from its weight to negligible levels [1]. The design lifetime of a reformer tube is typically 100,000 hours. However, most reformer operators use condition rather than time to determine when to replace a tube [2].

No standard specifications for the design requirements for HP alloy reformer tubes were found; however, a report released by the Nickel Development Institute lists the temperature and pressure range within which most reformer plants are designed to operate as well as the range of tube dimensions commonly used in the plants[3]. The operational temperature and pressure is typically within the range of 1652-1832°F and 218-435psi, with tube lengths varying between 33-46 feet. The inside diameter of the tubes ranges between 2-5 inches and the tube wall thickness commonly lies between 0.3-0.8 inches, depending on the specific temperature and pressure the plant is designed to operate at.

2.2: Development of HP Alloy

In the 1960's, the heat resistant (H) series of austenitic alloys were developed for use in reforming furnaces. The larger amount of chromium and nickel that these alloys contain increases the high temperature strength, ductility, and corrosion resistance during service [1]. The initial alloy used was the HK-40 alloy, which was improved with the addition of silicon and niobium in the early 1970's and finally replaced with the higher creep strength and oxidation resistance of the HP-mod alloy in the mid 1970's [3].

Eventually, this pursuit of increased creep strength and decreased weight has led to the industry acceptance of HP-micro, which contains additional elements in addition to the ones added to the HP-mod alloy.

2.3: Chemical Composition of HP Alloys

ASTM lists three official compositions for HP alloy steels, which are shown in Table 1. Standard A297 covers the basic, general usage HP alloy composition, while Standard A608 covers two different basic compositions adopted for use as centrifugally cast tubes in pressure applications at high temperatures. HP alloy tubes are rarely purchased with these standard chemistries, with the preference being for proprietary versions containing additional niobium and other micro-alloying elements to improve rupture properties [6]. These alternative HP alloys can be classified into two groups depending on the additional alloying elements. HP-modified alloys contain additional niobium while HP-microalloyed contains titanium, zirconium, and/or other alloying elements in addition to an increased amount of niobium [7].

Table 1. Standard HP compositions provided by ASTM Standards A297 and A608 [4][5].

Grade	Composition (wt%)								
	C	Mn	Si	P	S	Cr	Ni	Mo	Nb
HP[4]	0.35-0.75	2.00	2.50	0.04	0.04	24-28	33-37	0.50	---
HPNb[5]	0.38-0.45	0.50-1.50	0.50-1.50	0.03	0.03	24-27	34-37	0.50	0.50-1.50
HPNbS[5]	0.38-0.45	0.50-1.50	1.50-2.50	0.03	0.03	24-27	34-37	0.50	0.50-1.50

The addition of nickel to the HP alloys acts to stabilize and increase the amount of austenite in the tube, increasing the high temperature strength and stability from more common ferritic alloys. Chromium and silicon act to form protective oxides on the surface of the material to protect the tube from oxidation and the corrosive gases found in

the reforming process [8]. Carbide formers like niobium, titanium, tungsten, molybdenum, zirconium and vanadium, in addition to chromium, are used to form carbides in the material to increase the creep rupture strength by impeding the movement of dislocations. Titanium, niobium and tantalum are added to HP alloys in order to combine with carbon and nitrogen to prevent sensitization and intragranular corrosion susceptibility [6]. Sensitization occurs when carbides are precipitated at the grain boundaries, which can decrease the amount of corrosion inhibitors, like chromium, adjacent to the carbide making the depleted area more susceptible to corrosion. Intragranular corrosion is similar to sensitization, except the secondary carbide formation occurs inside the grains of the material. The secondary carbide precipitation is minimized in both cases by the addition of the corrosion inhibitors that combine with the carbon and nitrogen in place of the chromium and other corrosion inhibitors. Besides increasing oxidation resistance, the addition of silicon to the HP alloy also works to increase the casting fluidity and castability of the material [6].

2.4: Structure

The grain structure of the tube wall and the arrangement of the matrix-carbide structure are the two main elements of the HP alloy tubing that work to provide the strength, high temperature performance, and corrosion resistance necessary for use in the reforming process. The casting and machining process used to make the tube causes the grain structure found within the tube wall. The composition of the matrix and carbides within the alloy is a direct result of the alloying elements that make up the material composition as well as the temperature the tube experiences during service.

Because reformer tube alloys are not easily drawn or extruded, casting becomes necessary to produce the desired structures. Centrifugal casting is used because it produces an even structure with radial oriented grains that work to increase the strength and creep resistance of the tube [9]. The majority of centrifugally cast austenitic stainless steels used in the refinery industry are made up of a mixed and layered columnar-equiaxed grain structure [10]. As the molten metal is poured into the mold, a thin chill zone layer of fine equiaxed structure forms nearly instantaneously at the mold wall. Then a columnar zone of directionally oriented crystals perpendicular to the mold surface

forms adjacent to the chill zone. Finally, an equiaxed zone consisting of a large number of uniformly grown crystals can be formed next to the columnar zone at the inside diameter of the casting [11]. The ideal speed of mold rotation causes rapid adhesion of the molten metal to the mold wall with minimal vibration. This results in a casting with a uniform structure of continuous columnar grains through the thickness of the wall [10]. An increase in the mold rotation speed causes turbulence in the molten metal that shears off the tips of the dendrites and creates an equiaxed grain structure. Decreasing the mold rotational speed can also generate the equiaxed grain structure. In this case, the next layer of molten metal arrives after the previous layer solidifies into a distinct lap without any nucleation into the subsequent layer [10]. A large benefit of the centrifugal casting process is that castings tend to be produced with very few defects. Due to the centrifugal force and directional solidification of the casting, impurities and gas porosity are forced to the inner surface of the tube and then can be removed by machining [12]. The elongated and equiaxed fine grain structures produced by the centrifugal casting process work together to increase the durability of the tube. The elongated grains increase the creep resistance of the tube as well, while the fine grain interior structure works to resist carburization and other damaging reactions that occur within the reformer tubes [9].

The HP alloy microstructure consists of an austenite matrix with dendritic carbides and secondary carbides scattered throughout the matrix [7]. After casting, the carbide structure consists mainly of Cr_7C_3 formed along the grain and dendrite arm boundaries. During operating temperature exposure, this Cr_7C_3 structure then fully transforms to $Cr_{23}C_6$ with the formation of additional primary and secondary carbides [1]. In both the pre and post service conditions chromium and niobium carbides are the major precipitates with some additional titanium carbides [7].

2.5: HP Tube Service Performance

The performance of the HP alloy tubes is controlled by both the grain and carbide structures within the tube wall. As stated in Section 2.4, the grain structure of the HP tube wall typically consists of a thin layer of equiaxed grains at the outside diameter, followed by elongated radially oriented columnar grains and a thicker layer of equiaxed grains at the inside diameter. The equiaxed grain structure at the inside diameter works

to increase the resistance of the tube to creep crack propagation and carburization while the elongated columnar structure increases the creep resistance [1][9].

Working in conjunction with the grain structure, the carbides also serve to increase the creep strength and durability of the HP alloy tubing. The primary carbides work to prevent grain boundary sliding, while the secondary carbides act to resist dislocation motion [13]. During high temperature exposure (i.e. service exposure), the growth of the secondary carbides increases the resistance of the tube to creep deformation but decreases its toughness [1].

2.6: HP Tube Issues/Damage

There are several ways that the structural integrity of a centrifugally cast HP alloy tube used in the reforming process can be compromised including: casting defects, creep damage, changes to the carbide structure caused by high temperature exposure, and finally, damage resulting from exposure to the reforming process environment. Just one or even a combination of these defects limits the service life of reformer tubes and can potentially cause premature failure.

While the inner diameter of the cast tubes are machined to size to remove any possible crack propagating inclusions [1], issues resulting from the casting process can still occur. The simplest problem that can occur during the casting and the hardest to control is the variability of the grain structure, which can vary between castings as well as along the length of the tube [10]. This in turn causes variability in the creep performance throughout the tube, potentially making some sections more prone to creep failure, corrosion, etc. Due to the composition gradient adjacent to the crystals growing during solidification, the liquid zone in contact with the growing crystal has a lower purity. Under conditions of inadequate feeding this can cause the impure liquid to become trapped within the growing crystal wall and solidify, resulting in porous segregation zones [10]. Another issue with the tube castings is the variation in wall thickness that can occur along the length of the tube. This variation leads to non-uniform stress and temperature distributions along the length, possibly resulting in early failure of the tube.

The basic mechanism involved in causing creep damage is the generation of vacancies produced during the diffusion of species under stress and deformation on an

atomic scale. These vacancies tend to congregate on grain boundaries, causing a decrease in strength and the initiation and propagation of cracks [9]. For the HP tubes, the vacancies tend to collect at the precipitate/matrix interfaces, causing the formation of voids that then coalesce into cracks. The initiation of the voids initially occurs in association with the precipitates oriented perpendicular to the direction of the greatest applied stress [7]. In the case of reformer tubing, the greatest applied stress is perpendicular to the axis of the tube (also known as the hoop stress). The creep voids will initially form at the dendritic boundaries approximately one third of the wall thickness in from the inner surface, with the cracks first propagating to the inner diameter before expanding to the outer diameter [14]. There are five stages of increasing damage that are used to describe the formation of the creep voids and their subsequent evolution into cracks [14]. The first stage has no apparent void damage, with the second stage characterized by the appearance of isolated voids. In stage three, the isolated voids start to align and then combine into microcracks at stage four. Finally, stage five is characterized by the appearance of macrocracks in the tube wall.

In conjunction with the damage caused by creep, thermal history also serves to limit the service life of a tube. Thermal damage can be placed into two categories: microstructure change and thermal stress. Precipitation coarsening in the tube wall can occur at the temperature range in which reformer tubes operate. The coarsening occurs in order for the precipitates to minimize their surface energy, but it also causes them to release their trapped dislocations to relieve the stress caused by the volume change during precipitate growth [9][15]. The high temperature exposure also causes chromium depletion in the grain boundaries. However, the addition of carbide forming elements in the HP-micro alloy works to replace the chromium as carbide forming elements [1]. The temperature gradient that the HP reformer tubes experience affects service life through the introduction of non-uniform stresses both through the wall and along the length of the tube. Because the tubes are heated externally, the temperature at the outside diameter is greater than the temperature at the inside diameter. This causes a through wall stress gradient to form due to the differences in thermal expansion, and is especially prevalent near the bottom of the tube where the cooler reaction gas is injected. Both the microstructural transformation and thermal gradients combine to reduce the integrity of

the HP reformer tubes with the majority of premature failures being caused by localized overheating (such as catalyst collapse inside the tube disrupting the gas flow or burner misalignment) [16].

The main environmental damage that the HP reformer tubes need to withstand is carburization. An important concern when selecting materials for use in the petroleum industry, carburization occurs when the metal absorbs carbon from the environment which increases the formation of chromium carbides and reduces the creep strength while increasing the susceptibility towards oxide formation. This reduction in ductility makes the tube more susceptible to stress damage from thermal cycles or bending moments [3].

2.7: Evaluation Techniques

The methods used to evaluate HP tubing can be divided into the two different categories of nondestructive and destructive testing. As the names suggest, nondestructive testing can be performed without removing the tubes from service (though the plant still needs to be shut down) while destructive testing requires that the tubes be removed and sectioned for analysis. The most commonly used nondestructive techniques are diameter measurement, ultrasound, and eddy current evaluation. The destructive analysis consists of sectioning samples for microstructural analysis [17].

As a reformer tube experiences creep damage, the wall thickness of the tube will decrease as the tube bulges outward increasing the size of the outer diameter [2][17]. This means that the most damage will be concentrated in the thin region of the tube wall and allows the use of simple circumferential measurements, performed at specified distances (set by the plant operators) along the tube's length, to be used to calculate the outside diameter to detect any creep damage a tube may have experienced via a comparison to the as cast dimensions. Unfortunately, an increase in outer diameter is not necessarily an indicator of the presence of damage in the tube wall. Besides the obvious culprit of carbon deposit buildup on the tube wall from the heating process, the way the tube was machined can also adversely affect the diameter measurements. Slight miscalculations made during the machining of the inside diameter of the tube can cause the cut hole to deviate off center, causing a significant reduction in wall thickness on one side with

excess material on the other [2]. This means that it's possible for the tube to fail on the thin wall side while showing little if any change in the outer diameter.

Ultrasonic testing uses high frequency sound waves to analyze parts and materials. Some of the uses more pertinent to the evaluation of HP alloy reformer tubing include wall thickness measurements and detection of cracks and voids. Measuring the difference in energy as well as the travel time between the reflected and incident waves can identify the location and type of flaw. The main two issues that ultrasound faces is that surface needs to be smooth and defects oriented parallel to the sound wave are sometimes not detected. If the surface is too rough, air underneath the ultrasound transducer can block the passage of the wave. Defects oriented parallel to the sound wave and with small enough cross sections can go undetected by not reflecting enough of the incident beam to allow for detection.

Eddy current testing measures changes in a magnetic field induced in the tube to detect cracks and other flaws near the surface of the outer diameter. The magnetic field in the tube is generated from an alternating current passing through a conducting coil placed around the tube. The alternating current passing through the coil produces a magnetic field; which then causes an electrical current to flow in closed loops within the tube called eddy currents. These eddy currents then cause the production of the magnetic field in the tube wall, which magnetic sensors measure to characterize the tube. The main issue with eddy current evaluation is that the penetration depth is limited, primarily controlled by the frequency of the current and the conductivity and permeability of the tube [2]. Microcracks from the void coalescence propagate to the internal diameter first, potentially causing damage to go unnoticed [14]. In addition, alloys containing a high percentage of nickel, like the HP tubing, require the use of magnetically shielded or biased coils to reduce the effects of material permeability variations [2].

Unlike the other three previously mentioned techniques, microstructural analysis requires that the tubes be removed from service and sectioned for viewing. For a full microstructural analysis, a series of ring samples cut from the same tube need to be obtained and evaluated because the creep damage is rarely distributed evenly around the complete cross section [14]. Four levels are used to evaluate microstructural damage [18]. At level A some isolated damage is observable, indicating approximately one third of the

life has been used. The damage centers align at level B and microcracks form between them at level C, corresponding to one half and two thirds of life used respectively. Finally, the tube can be considered unfit for service when it reaches level D where the microcracks and aligned damage centers extend through sixty percent of the tube wall. The main source of error for microstructural evaluations is the variability of damage in the tube. The actual size and number of voids and microcracks can be subject to large variations and may bear little relation to the actual size of open volumes in the material [19].

3: Objectives

The ultimate goal of this project is to use the ex-service samples and creep tested samples to correlate the formation of voids within the samples with the size and distribution of their grains as well as chemical composition. This information is then used to determine if there is a possible composition/grain distribution that minimizes void formation during service. If so, the results could then be used to help determine the lifetimes of HP tubes currently in service and to aid in the design of future reforming tubes.

4: Experimental Procedures

4.1: Service Exposed Wall Thickness Evaluation

The wall thickness of the eight HP alloy tube ring sections was evaluated upon their delivery. The samples were marked in one inch increments along their outer walls with two reference marks, one on either side. The inner and outer diameters of these ring sections were then traced on paper, with the reference marks clearly shown as well as the marks at one inch increments. The tube sections were then measured at the one-inch increments, using a micrometer with a pin anvil. Each of the measurements was then recorded alongside the marks on the trace of the ring section. Upon completion of the thickness evaluation of each tube, the measurements were evaluated for maximum thickness, minimum thickness, average thickness, and the percent difference between the maximum and minimum thicknesses. The thickest section of the tube wall was marked for further evaluation as it was most likely the area that experienced the least amount of void swelling; thus giving the best contrast when compared against the creep tested samples.

4.2: Sectioning of Samples

Two different sample types were sectioned for the evaluation of the HP alloy tubes. The ring samples were sectioned to view the circumferential and longitudinal structure of the tubes as well as to provide samples for chemical analysis. Creep-tested samples, testing both the circumferential and longitudinal directions of each of the tubes, arrived after the ring samples and needed to be sectioned to achieve the same longitudinal and circumferential views as the ex-service samples. The creep samples were from different sections of the HP tubes than the ring samples.

4.2.1: Service Exposed Samples

Sections of approximately two inches in length were removed from the thickest section of the tube ring using a crosscut saw equipped with an abrasive wheel. These sections were then cut in half through the wall thickness. One half was set aside for

analysis of the tube ring sample along the circumferential direction, while the other was sectioned further.

The second section was used to make the sample for chemical analysis as well as the sample for analysis of the ring section along the transverse direction in relation to the tube. It was sectioned with a computerized abrasive saw for increased precision. The chemical analysis tests required a flat-sided sample with a surface area of at least one square inch. The first two cuts were to remove the through-wall ends of the sample to create two faces parallel to each other and perpendicular to the outer faces of the ring. One of these pieces was mounted to view the longitudinal direction of the tube. The next cut was to remove the concave curve of the sample caused be the ID. Finally, the last cut removed the convex curve caused by the OD. These cuts resulted in a rectangular sample with 90 degree corners and a surface area of two of the sides over one square inch.

4.2.2: Creep Tested Samples

The creep-tested samples were sectioned for circumferential and longitudinal views like the service-exposed samples. Each sample had the grips removed and was then transversely sectioned across the center of the gauge length. This produced two halves of the gauge length for analysis. One of the halves was sectioned through the ID and OD with the cut running through the center of the thickness of the sample. The other half had a 3-5mm slice removed, transverse to the pull direction across the gauge width, to view the sample across the center of the gauge.

4.3: Chemistry Analysis

Chemistry sections sectioned from the service-exposed samples were sent off to Alstom (an industrial laboratory) in Chattanooga, TN, for chemical analysis. The target elements were carbon, manganese, phosphorus, sulfur, silicon, nickel, chromium, molybdenum, vanadium, niobium, titanium, cobalt, copper, aluminum, tungsten, arsenic, tin, zirconium, lead, nitrogen, oxygen, and zinc. The majority of the elements were detected using optical emission spectroscopy, while combustion infrared detection was used for carbon and sulfur analysis and inert gas fusion detection was used for the oxygen

and nitrogen analysis. The results for the chemical analysis on each of the tubes were compared to the standard composition outlined in the ASTM standard A608.

Optical emission spectroscopy is a technique that analyzes the excitation of atoms energized by a spark provided by an electrode. The excitation of the electrons of the atoms releases energy, which is then analyzed as a spectral pattern by the machine. Combustion infrared detection uses a furnace to heat up the sample in a pure oxygen environment. It then analyzes the released gases (such as CO, CO_2 and SO_2) to determine the amount of carbon and sulfur. Finally, inert gas fusion detection heats up the sample in an inert atmosphere and analyzes the gas released from the sample (in this case O_2 and N_2).

4.4: Mounting, Grinding and Polishing

Before mounting, each sample had an electric lead (for electrolytic etching) approximately three inches long spot-welded opposite the evaluated face. A hole was then punched in an appropriately sized (just large enough in diameter to contain the sample) disposable mounting tin at the height of the electric lead to prevent the free end of the lead from being mounted with the sample. After the hole was punched, the sample was inserted into the tin with the lead running out of the punched hole. Superglue was used to adhere the evaluated face to the bottom of the tin to prevent movement while mounting, as well as to seal the hole around the lead.

After the superglue dried in the glue-mounted samples, an appropriate amount of two-part epoxy for the amount of samples was mixed for mounting. As the epoxy and hardener were mixed together, a small amount of black spray paint was added to increase the contrast between the epoxy and mounted sample. Once the epoxy and paint was fully mixed, it was carefully poured into the tin mounted samples to within approximately 0.25 inches from the top of the tin. After pouring, the tins were placed into a sealed chamber and had a vacuum applied to them in order to remove any bubbles from the epoxy mounts. The samples were removed from the vacuum chamber once the bubbles had been removed and left to solidify for the time specified by the epoxy directions before removal from the tins. Upon removal, each of the samples was labeled on the side of the epoxy mount using a handheld scriber.

Each of the mounted HP samples were wet-ground and then polished using a motorized six-inch grinding/polishing wheel and adhesive pads. The grinding process progressed from 240 to 400 and finally to 600 grit before moving on to the polishing stage. The samples were held at each grinding stage until the generated scratches were uniform across the entire face of the sample and running parallel to the direction of the rotation of the grinding pad. Between grinding steps, the samples were rinsed in water and then methanol before being blown dry, using a heated dryer, in order to remove any residual grit from the previous step. Upon moving to the next step, the samples were rotated 90 degrees in order to remove the scratches generated by the prior step.

After the 600 grit grinding stage has been completed and the samples had been cleaned and dried, they were polished using 0.05-micron alumina powder and a six-inch adhesive backed felt pad, applied to the grinding wheel. The alumina powder as mixed into a slurry with distilled water in a squirt bottle and then applied to saturate the felt pad on the grinding wheel. The samples were moved around the felt pad counter to the direction of rotation of the wheel for approximately 1.5 minutes, or until there were no observable scratches on the face of the sample. After being cleaned and dried, the samples were checked again for scratches using an optical microscope up to 400X magnification. If significant scratching is detected at 400X, the polishing step was repeated until the scratches had been removed. The samples were then stored in a desiccator after polishing in order to protect the polished surface from oxidation, scratching, or any other damage.

4.5: Microstructure Evaluation

The microstructure evaluation provided the majority of the information for the project. The samples were electrolytically etched and then evaluated using both optical light microscopy and scanning electron microscopy. The data gathered from these two techniques was used to analyze the microstructure, phase composition, and volume percent voids of the samples.

4.5.1: Microetching and Imaging

The polished samples needed to be etched to fully reveal the microstructure for evaluation. The etching was accomplished using an aqueous solution of 10% oxalic acid and a DC power supply with adjustable voltage to electrolytically etch each sample. The oxalic acid solution was poured into a Pyrex crystallizing dish to a great enough depth to completely cover the samples when the mounts are placed on their side. The DC power supply was then set to 2.0 volts with the red (positive) electrode attached to the lead joined to the sample and black (negative) electrode attached to a stainless steel rod approximately 5 inches long.

Making sure to keep the positive electrode out of the oxalic acid solution, the samples were placed in the dish on their side with their back against the wall of the dish and their polished face facing towards the center. Once this was accomplished, the voltage output of the power supply was turned on and the stainless steel electrode was lowered into the solution two inches away from the polished face of the sample. At an even rate, the stainless steel electrode was then moved back and forth parallel to and evenly across the face of the samples for approximately eight seconds. After that, the electrode was removed and the voltage output turned off. The samples were then taken out of the solution, the positive lead removed, and then rinsed off with deionized water and then methanol. After the methanol rinse, the samples were air dried with a heated air dryer and then had the etch checked by optical microscopy to ensure that the structure has been appropriately outlined. If more contrast turned out to be necessary, the etching was repeated in one-second increments, being careful not to over etch. Over etching was found to cause the carbides to fall out of the samples, necessitating regrinding and polishing to remove the over etched layer.

After the samples had been successfully etched, they were marked using a micro hardness indenter just inside the ID and OD as well as at the center of thickness of each sample. These served as reference points for the images. For the service-exposed samples, the marks were made at approximately the center of the width of the polished sample face. The creep-tested samples were marked just inside the center of the gauge length and at the fillet of the sample.

The marked samples were then imaged using an optical light microscope (OLM) at 50 and 500X magnification, at each of the designated locations, for microstructural evaluation. In addition, five images randomly arranged around each mark were obtained at 100X magnification to be used in the void evaluation.

4.5.2: SEM/EDS Evaluation

Two samples from each manufacturer, one service exposed and one creep tested, were imaged at 500, 1000, 1500, and 3000X magnification using a scanning electron microscope (SEM). Furthermore, energy dispersive x-ray spectroscopy (EDS) was used to identify the composition of the phases/structures observed during the SEM imaging. Magnification on the SEM needed to be increased to 20,000X or higher during EDS evaluation in order to ensure that the targeted areas were analyzed.

4.5.3: Void Evaluation

The 100X micrographs obtained during the OLM analysis were evaluated for voids using the point counting method outlined in the ASTM Standard E562-11 [20]. A ten thousand-point grid was laid over each image and the voids were counted and evaluated according to the standard. The resulting volume percent void measurements were then used to compare the service-exposed samples against each other as well as with their creep tested samples.

4.6: Macrostructure Evaluation

After the microstructure analysis had been completed, photo macrographs of the samples were used to analyze the grain structures of the service exposed samples. In order to view the grain structure, a new etchant needed to be applied to the samples on top of the etchant used to reveal the microstructure. After imaging with a conventional camera, the images were then analyzed to identify the grain structure and to calculate the amount of fine grains present within the sample wall.

4.6.1: Macroetching and Imaging

Lepito's etchant was used to reveal the grain structure of the samples for macrostructure analysis. Using a pair of tongs, a cotton balls were soaked in the etchant and then applied uniformly to the surface of the samples for about 20 seconds. After the 20 seconds, the samples were rinsed off with deionized water followed by methanol and then dried with a heated air dryer. If additional etching was required, the procedure was repeated in three second intervals until the desired contrast was achieved.

The images of the macro etched samples were obtained with a standard DSLR (digital single lens reflex) camera with a 60mm f/2.8 macro lens (maximum aperture width of 21.4 mm). In addition to the specialized macro lens, a light box was used to provide additional illumination on the sample surface. After an image on the sample was obtained, the digital image was processed with photo editing software in order to remove the background and to adjust the contrast and brightness to allow for maximum visibility of the grain structure.

4.6.2: Percent Fine Grain Evaluation

The longitudinal photo macrographs of the service-exposed samples were analyzed to calculate the amount of fine grains in the tube walls. The thickness of the fine grain region was measured and then divided by the overall thickness of the tube wall. This yielded the fractional amount of fine grains in the wall of the tube.

5: Sample Summary

In total, this project analyzed eight different HP alloy tube samples and eighteen creep tested dog bone specimens (two creep tests were repeated with different samples). Each of these twenty-six specimens were sectioned following the procedures outlined above, increasing the total number of samples to 52 in all. Figure 1 shows an example of the labeling key used for identifying the samples while Table 2 contains a breakdown of the sanitized sample designations and lists the general information provided for each of the tubes.

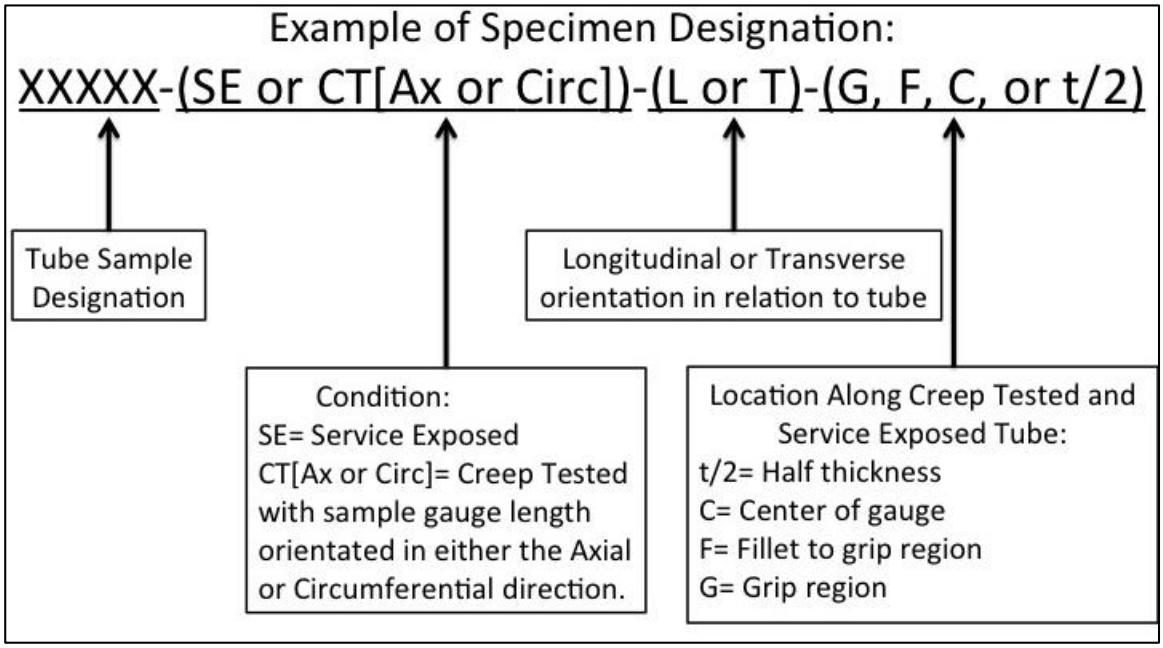

Figure 1. Labeling key used to identify samples.

Table 2. Tube sample designation breakdown and general information provided by the project sponsor for each of the tubes.

Sample:	Plant:	Manufacturer:	Tube Segment Elevation (ft)[1]:	Design Pressure (psig):	Operating Pressure (psig):	Design Temperature (°F):	Operating Temperature (°F):	Design Life (hrs):	Operational Lifetime (years):	Comments:
1M1P1	P1	M1	0 to 2	590	520	1755	1682	100000	19	No comment
2M1P1	P1	M1	0 to 2	590	520	1755	1696	100000	19	No comment
3M2P2	P2	M2	10 to 14	540	460	1745	1648	200000	12	Inspection found eddy current indications at this elevation.
4M3P3	P3	M3	4 to 6	620	540	1740	1658	200000	17	Neighboring tube ruptured 3"-9" above floor
5M3P3	P3	M3	4 to 6	620	540	1740	1662	200000	17	End of row tube similar to the failed tube.
6M3P4	P4	M3	0 to 2	620	545	1740	1615	200000	16	No comment
7M3P4	P4	M3	0 to 2	620	545	1740	1620	200000	16	No comment
8M3P5	P5	M3	8 to 10	440	390	1710	1650	200000	16	Tube ruptured 3"-8" above floor.

Notes:

[1]: Elevation is relative to reformer floor being 0 ft elevation and progressing upward. In general, tube is predicted to be hottest near the reformer floor.

[2]: All tubes segments are fabricated from centrifugally cast HP microalloyed base metal.

6: Results and Discussion

All of the procedures outlined in Section 4 were accomplished successfully. Each of the ex-service samples was dimensioned for wall thickness then sectioned for chemistry analysis and mounting for imaging. The creep tested ex-service samples were all sectioned and mounted for imaging. All of the mounted samples were optically imaged to view the grain and carbide structures as well as to perform void counts. Because of time constraints, one ex-service and one creep tested sample from each of the three manufacturers was imaged and analyzed with EDS on the SEM.

6.1: Wall Thickness Measurements

A summary of the results from the wall thickness measurements is listed in Table 3 below. As is shown, there is quite range of wall thickness variation between the different tube ring samples ranging from 0.011 inches for sample 2M1P1 to 0.046 inches for sample 4M3P3. Comparing tubes from the same manufacturer and plant (tubes 4M3P3 and 5M3P3 and tubes 6M3P4 and 7M3P4) indicates a small amount of variation, on the scale of less than a hundredth of an inch, in the wall thickness deviation. However, tubes 1M1P1 and 2M1P1 do not follow this trend, with the variation in the wall thickness deviation being over thirty thousandths of an inch. While this comparatively large variation could be an indicator of difference in casting or creep damage, further evaluation and comparison will be done in the subsequent evaluation sections.

Table 3. Results of wall thickness measurements of HP alloy tube ring sections.

Tube Sample	Average Wall Thickness (in)	Minimum Wall Thickness (in)	Maximum Wall Thickness (in)	Difference Between Max. and Min. Wall Thicknesses (in)
1M1P1	0.565	0.547	0.591	0.044
2M1P1	0.538	0.534	0.545	0.011
3M2P2	0.777	0.771	0.787	0.016
4M3P3	0.573	0.552	0.598	0.046
5M3P3	0.568	0.548	0.588	0.040
6M3P4	0.591	0.582	0.601	0.019
7M3P4	0.621	0.609	0.633	0.024
8M3P5	0.498	0.485	0.510	0.025

6.2: Chemistry Composition Analysis

Table 4 presents a complete list of the chemistries for the ex-service samples (measured by Alstom in Chattanooga, TN) in comparison to chemistry of a sample (A288) previously examined in an earlier HP microalloy material [7]. ASTM chemistries for Standards A297 [4] and A608 [5] are also included. Due to the large numbers of alloying elements, all of the tube samples in addition to sample A288 can effectively be classified as microalloyed HP alloys. Comparing the reported chemistries to the two ASTM standards reveals that the ex-service HP alloy samples follow the composition listed for HPNb in ASTM A608 while sample A288 from the previous study follows the composition listed for HPNbS in the same standard. It is to be expected that the cast HP alloy samples follow ASTM A608 and not ASTM A297 because ASTM A608 designates specifications for centrifugally cast tubing rather than the general casting specification listed as ASTM A297. The only difference between the compositions listed in ASTM A608 is that HPNbS contains 1.50-2.50 wt.% silicon while HPNb contains 0.50-1.50 wt.% silicon. In addition to an increased amount of silicon, the only other significant compositional difference sample A288 has when compared to the ex-service samples is that it contains a greater amount of phosphorous and a decreased amount of molybdenum.

By comparing the ex-service samples listed in Table 4, a significant difference can be shown between the tubes from manufacturer M1 (1M1P1 and 2M1P1) and the tubes from manufacturers M2 and M3. The ex-service tubes produced by M1 have a much higher weight percent of carbon than the tubes from the other manufacturers and have a decreased amount of silicon, niobium, titanium and aluminum. In addition, only tubes 8M3P5 and 3M2P2 have a manganese content as low as the tubes from manufacturer M1; with tube 3M2P2 also having a decreased amount of tungsten similar to the M1 samples.

Table 4. Chemistry results for the ex-service HP tube samples, sample A288 from a previous study [7], and the compositions provided by ASTM Standards A297 [4] and A608 [5].

Sample												
Designation	1M1P1	2M1P1	3M2P2	4M3P3	5M3P3	6M3P4	7M3P4	8M3P5	Sample A288	HP-ASTM A297	HPNb-ASTM A608	HPNbS-ASTM A608
Manufacturer	M1	M1	M2	M3	M3	M3	M3	M3				
Plant of Origin	P1	P1	P2	P3	P3	P4	P4	P5				
Chemistry Results (wt%)												
Carbon	0.544	0.612	0.456	0.450	0.450	0.474	0.465	0.460	0.40	0.35–0.75	0.38–0.45	0.38–0.45
Manganese	0.57	0.72	0.58	1.01	1.02	1.02	1.11	0.49	1.030	2	0.50–1.50	0.50–1.50
Phosphorus	0.015	0.012	0.018	0.019	0.019	0.020	0.019	0.018	0.051	0.040	0.030	0.030
Sulfur	0.008	0.006	0.006	0.008	0.007	0.004	0.008	0.006	0.008	0.04	0.03	0.03
Silicon	0.65	0.90	1.02	1.46	1.56	1.50	1.51	1.35	2.040	2.50	0.50–1.50	1.50–2.50
Nickel	35.92	37.84	36.52	35.34	34.59	35.95	34.44	34.47	35.80	---	---	---
Chromium	25.59	24.96	26.28	24.32	24.82	24.46	25.01	25.42	24.62	24–28	24–27	24–27
Molybdenum	0.076	0.031	0.034	0.043	0.038	0.041	0.049	0.034	<0.01	0.5	0.5	0.5
Vanadium	0.177	0.207	0.158	0.213	0.069	0.217	0.075	0.073	0.030	---	---	---
Niobium	0.49	0.46	0.82	0.95	1.07	0.98	1.09	0.77	0.700	---	0.50–1.50	0.50–1.50
Titanium	0.030	0.032	0.117	0.101	0.085	0.109	0.082	0.129	0.130	---	---	---
Cobalt	0.076	0.048	0.033	0.034	0.035	0.074	0.083	0.048	0.03	---	---	---
Copper	0.07	0.02	0.03	0.09	0.09	0.05	0.04	0.03	0.010	---	---	---
Aluminum	0.011	0.010	0.041	0.043	0.034	0.041	0.097	0.032	0.010	---	---	---
Tungsten	0.06	0.01	0.01	0.91	0.88	0.93	0.90	0.77	0.020	---	---	---
Arsenic	<0.001	<0.001	<0.001	>0.001	<0.001	<0.001	<0.001	<0.001	0.001	---	---	---
Tin	0.003	0.003	0.004	0.007	0.008	0.006	0.005	0.005	0.001	---	---	---
Zirconium	<0.001	<0.001	0.001	0.018	0.003	<0.001	0.004	0.056	0.04	---	---	---
Lead	<0.001	<0.001	<0.001	<0.001	<0.001	<0.001	<0.001	<0.001	0	---	---	---
Nitrogen	0.107	0.064	0.028	0.048	0.049	0.057	0.063	0.058	0.034	---	---	---
Oxygen	0.007	0.008	0.002	0.002	0.002	0.002	0.001	0.001	0.003	---	---	---
Zinc	<0.001	<0.001	<0.001	<0.001	<0.001	<0.001	<0.001	<0.001	0.001	---	---	---

6.3: Microstructure Comparison

Figure 2 shows the effect that elevated temperature exposure (at 1950°F for 953.1 hrs. during creep testing) has on the microstructure of an HP microalloy sample (specifically sample A288 from the previous HP alloy study [7]). Both OLM micrographs were originally obtained at 1000X magnification, with no scale bars being provided in the previous report. Image b of Figure 2 was obtained away from the gauge length in the grip of the sample. Figures 3-14 show the ex-service and creep tested microstructures for service exposed tubes from each of the manufacturers. The micrographs in Figures 3, 5, 7, 9, 11, and 13 were obtained using optical light microscopy while the images in Figures 4, 6, 8, 10, 12, and 14 were obtained using scanning electron microscopy. It is important to note that the contrast in the SEM micrographs is different from the OLM micrographs (specifically, in this case, the contrasts are reversed). The reason for the contrast difference between the optical and SEM images is that while an optical microscope detects reflected light from the sample the SEM bombards the sample with an electron beam and analyzes the emitted and reflected electrons to generate an image. This causes the SEM micrograph to be influenced by the ability of the target area to absorb and/or reflect electrons rather than light, which generates grey scale images with contrasts different from those obtained using an OLM.

The microstructure of HP alloy A288 changed quite dramatically from the as-cast condition after exposure to elevated temperatures during creep testing as is illustrated in Figure 2. The as-cast condition of sample A288 consists of an austenitic matrix with carbides that appear both elongated and as distinct particles. After elevated temperature exposure to 1950°F, the carbides become more globular in shape and secondary carbides precipitate in the matrix. In addition two different carbides appear within the original primary carbides, replacing the previously uniform as-cast condition. The ex-service service and creep tested samples appear to follow this trend, with the micrographs of the ex-service samples closely matching sample A288 after it experienced a prolonged exposure to elevated temperatures during creep testing. By comparing the micrographs of the three different service exposed tubes (Figures 3-14), it can be seen that the extent of precipitation of secondary carbides is significantly greater in tubes 1M1P1 and 3M2P2

than in tube 4M3P3. The microstructure of the service exposed and creep tested samples does not appear to vary from that of the service exposed condition.

While the samples were being imaged in the SEM (Figures 4, 6, 8, 10, 12, and 14), the compositions of the light and dark carbides were analyzed with EDS to aid in their identification. The results, listed in Tables 3-5, show the darker colored type I carbides as containing mostly chromium with some iron, nickel and tungsten. The lighter colored type II carbides were determined to contain niobium, chromium, iron and nickel. It must also be noted that the amount of niobium and chromium in their respective carbides increased after creep testing. According to the EDS data, the dendrite core region is composed mainly of chromium, iron and nickel. The detection of iron and nickel in both the type I and II carbides is due to the energizing electron beam energizing the matrix background in addition to the targeted carbide. This inadvertent energizing of non-target areas also causes the detection of chromium in the light carbides because they occur in close proximity to the dark carbides, which are rich in chromium. While detected, the amounts of carbon and several other lighter elements in the target areas are not deemed to be accurate due to the lack of sensitivity in the EDS detector used for this analysis. Overall, the EDS data indicates that the dark globular carbides in the SEM images are mainly chromium carbides while the white globular carbides are mainly niobium carbides. After casting, the carbide structure of HP alloys consists mainly of Cr_7C_3, fully transforming into $Cr_{23}C_6$ with additional primary and secondary carbides after operating temperature exposure [1].

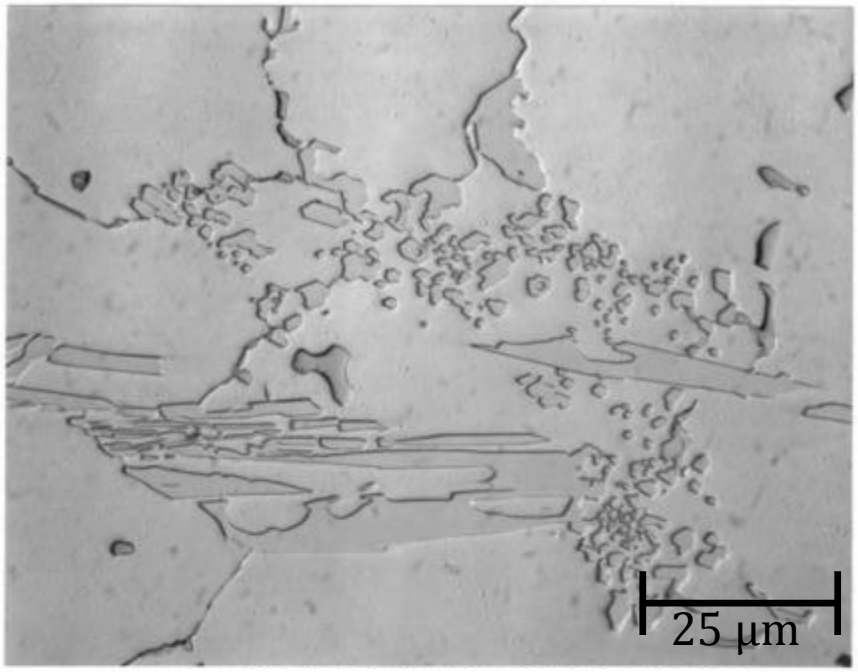

a. As-cast condition

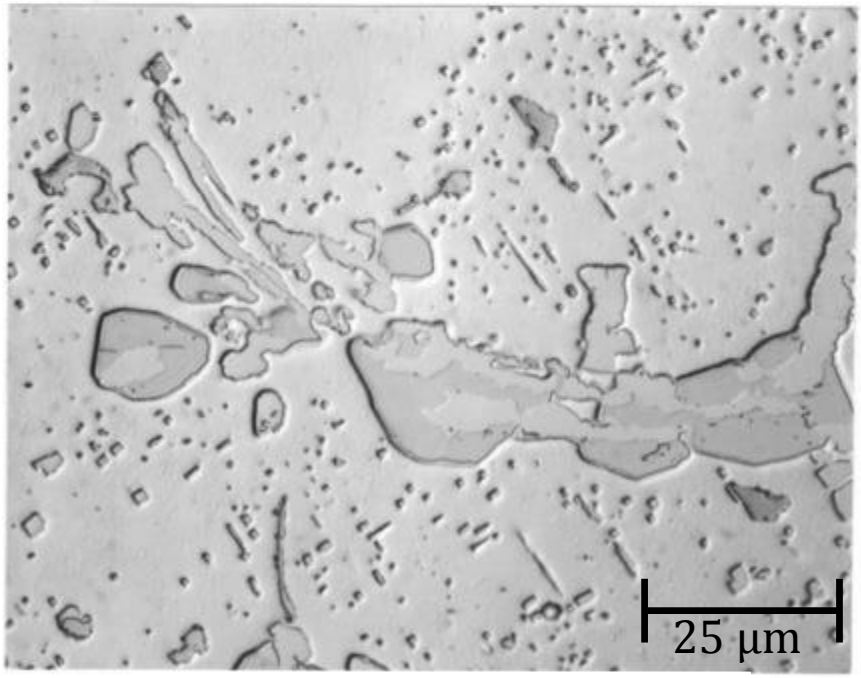

b. After elevated temperature exposure

Figure 2. OLM micrographs of microalloyed HP sample A288 obtained from a previous project [1] 1000X magnification. Image a is of the as-cast microstructure while image b is from the grip of the creep sample after testing at 1950°F for 953.1 hrs.

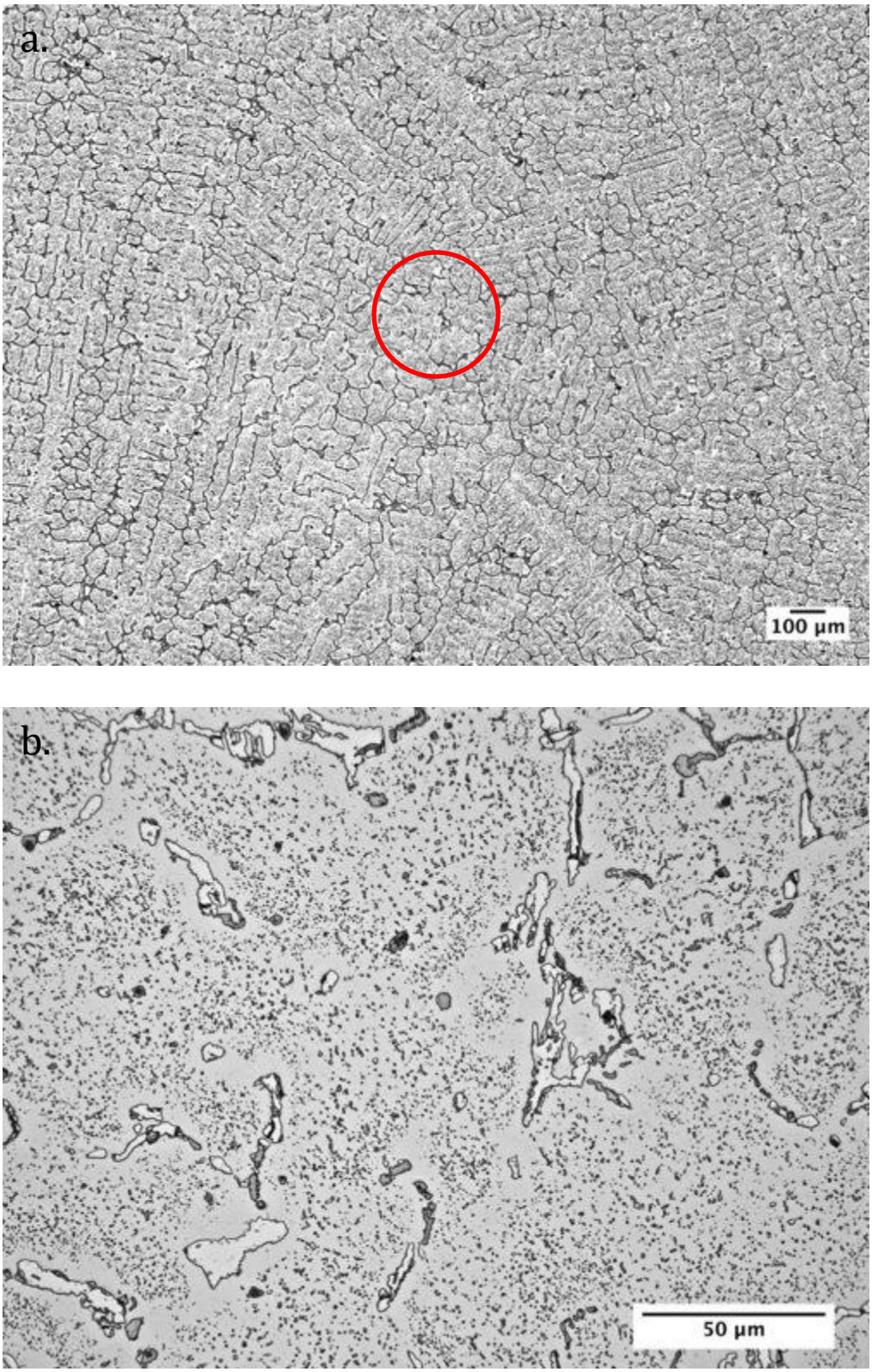

Figure 3. HP tube 1M1P1-SE OLM micrographs at a) 27.5X and b) 275X printed magnification.

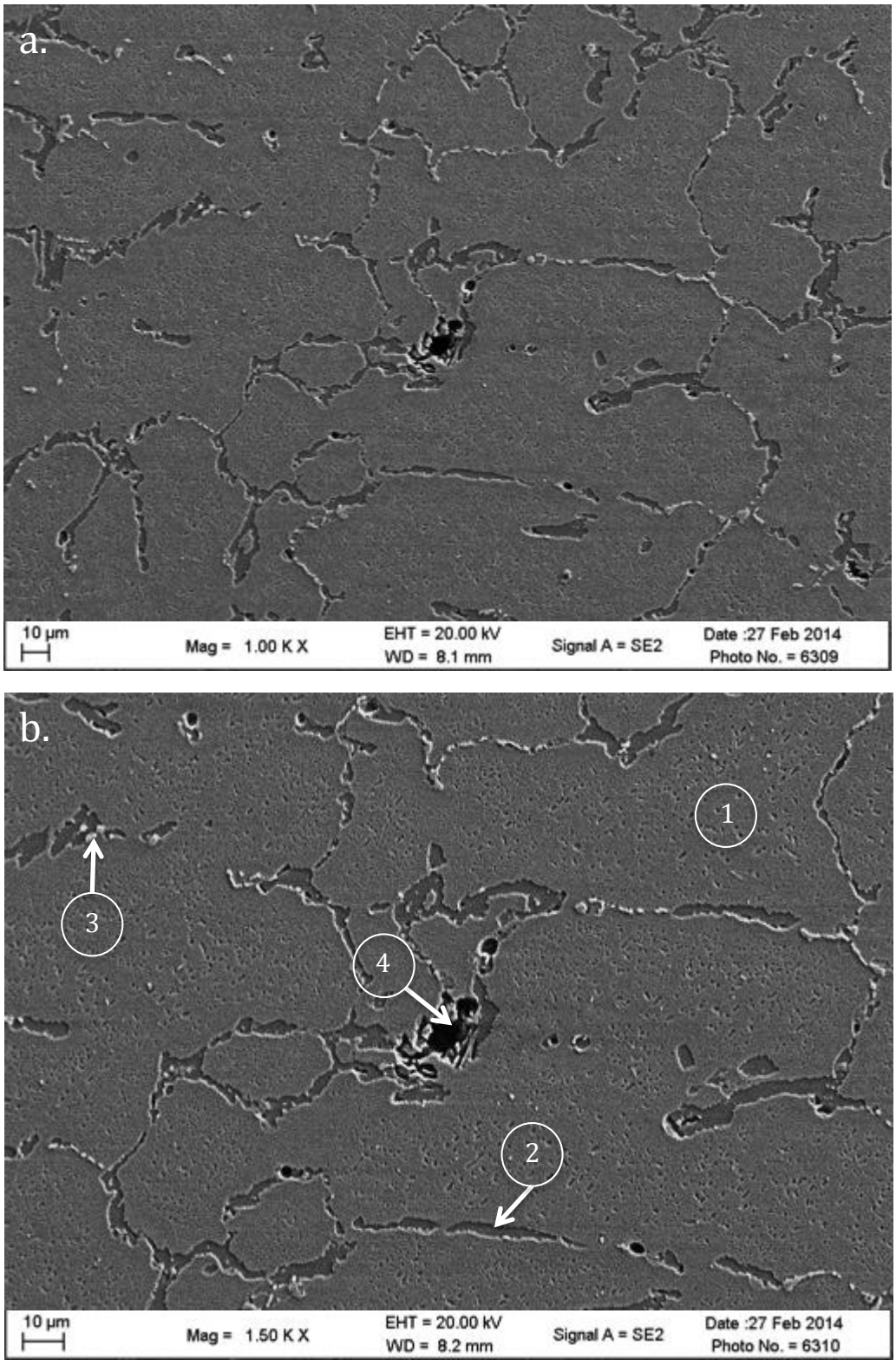

Figure 4. HP tube sample 1M1P1-SE SEM micrographs at a) 550X and b) 825X printed magnification. The marked areas in image b are examples of 1: the dendrite core region with secondary precipitates, 2: a type I carbide, 3: a type II carbide, and 4: a void.

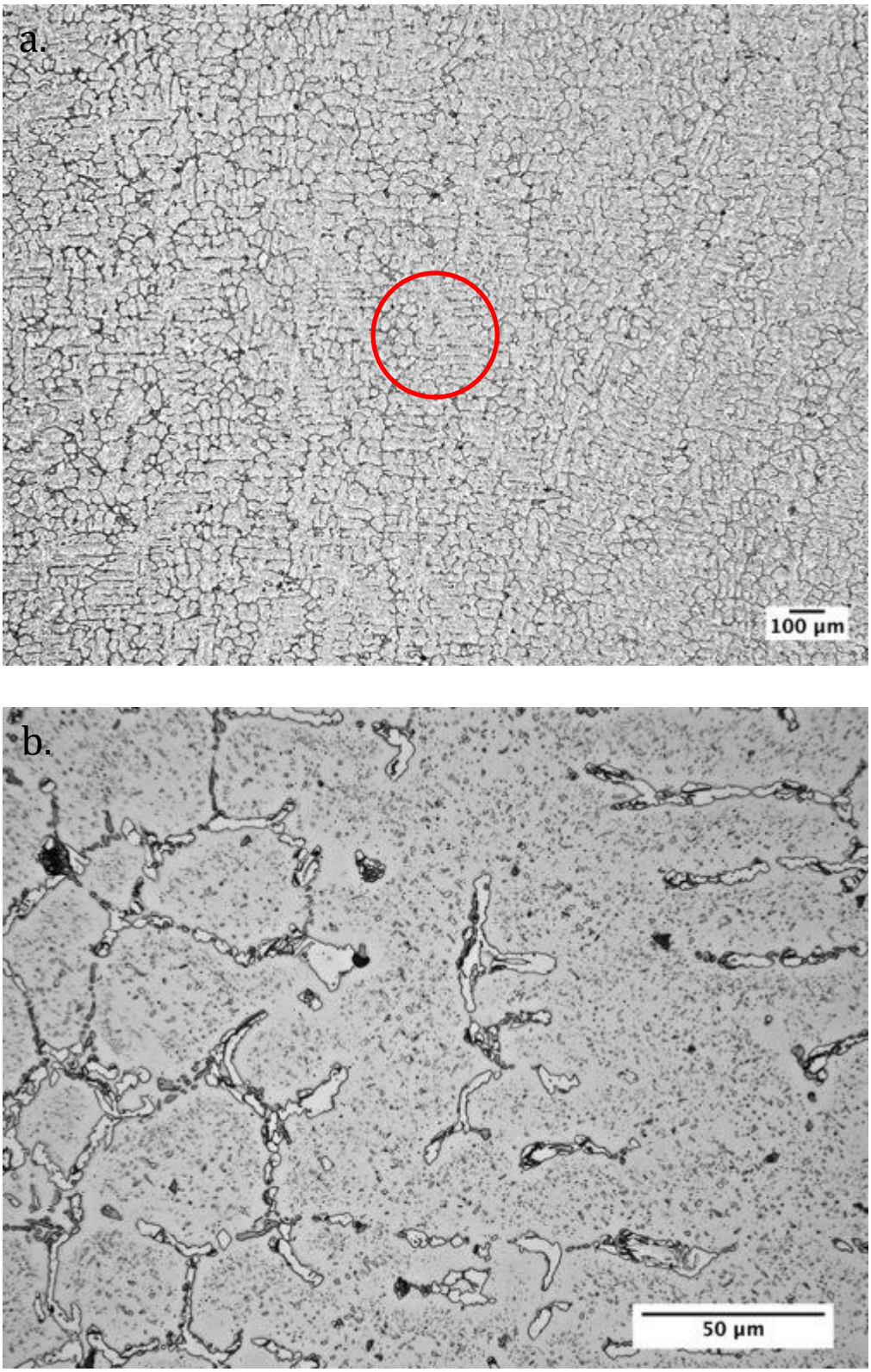

Figure 5. HP tube sample 1M1P1-CT[Ax] OLM micrographs at a) 27.5X and b) 275X printed magnification.

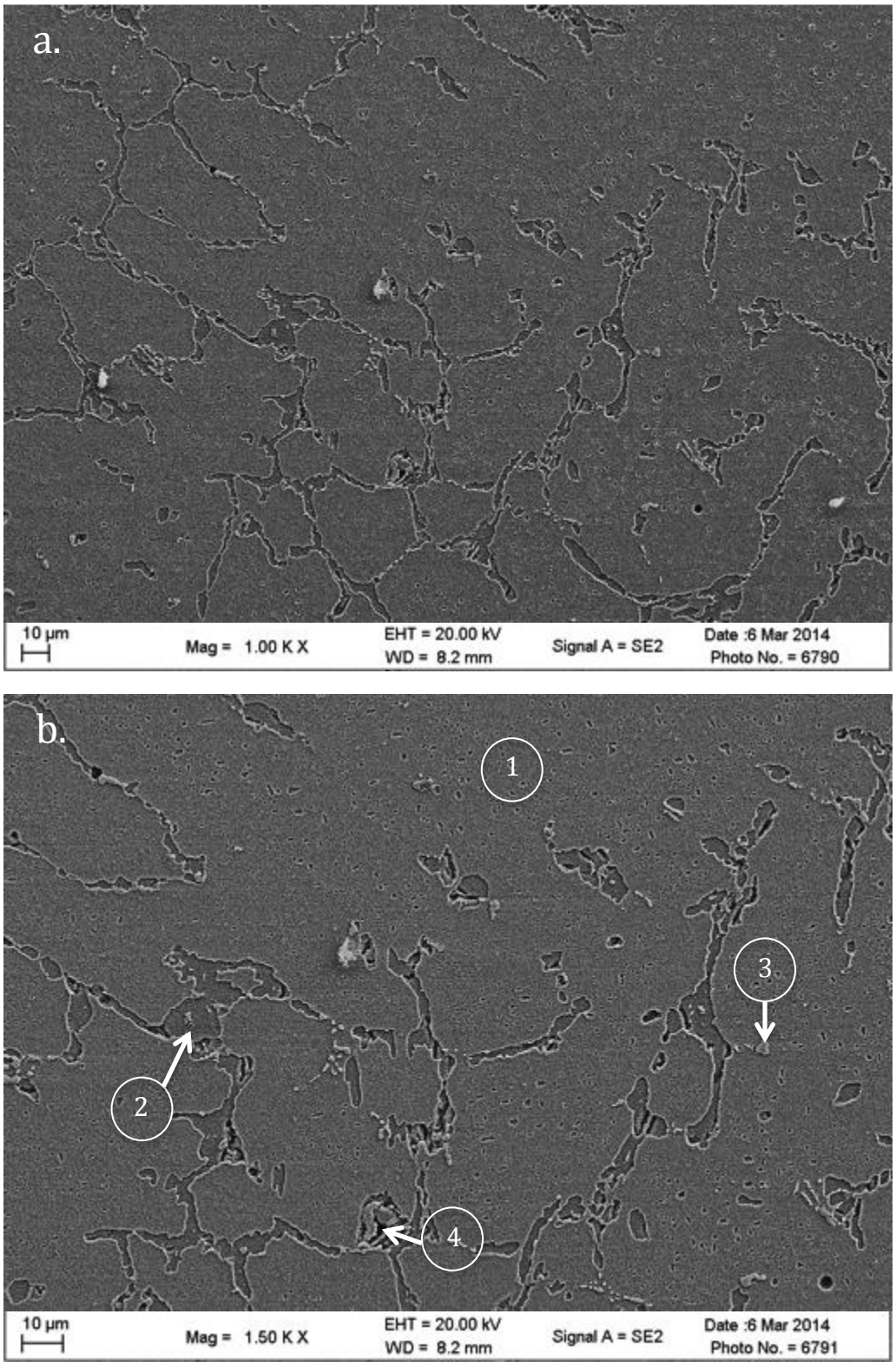

Figure 6. HP tube sample 1M1P1-CT[Ax] SEM micrographs at a) 550X and b) 825X printed magnification. The marked areas in image b are examples of 1: the dendrite core region with secondary precipitates, 2: a type I carbide, 3: a type II carbide, and 4: a void.

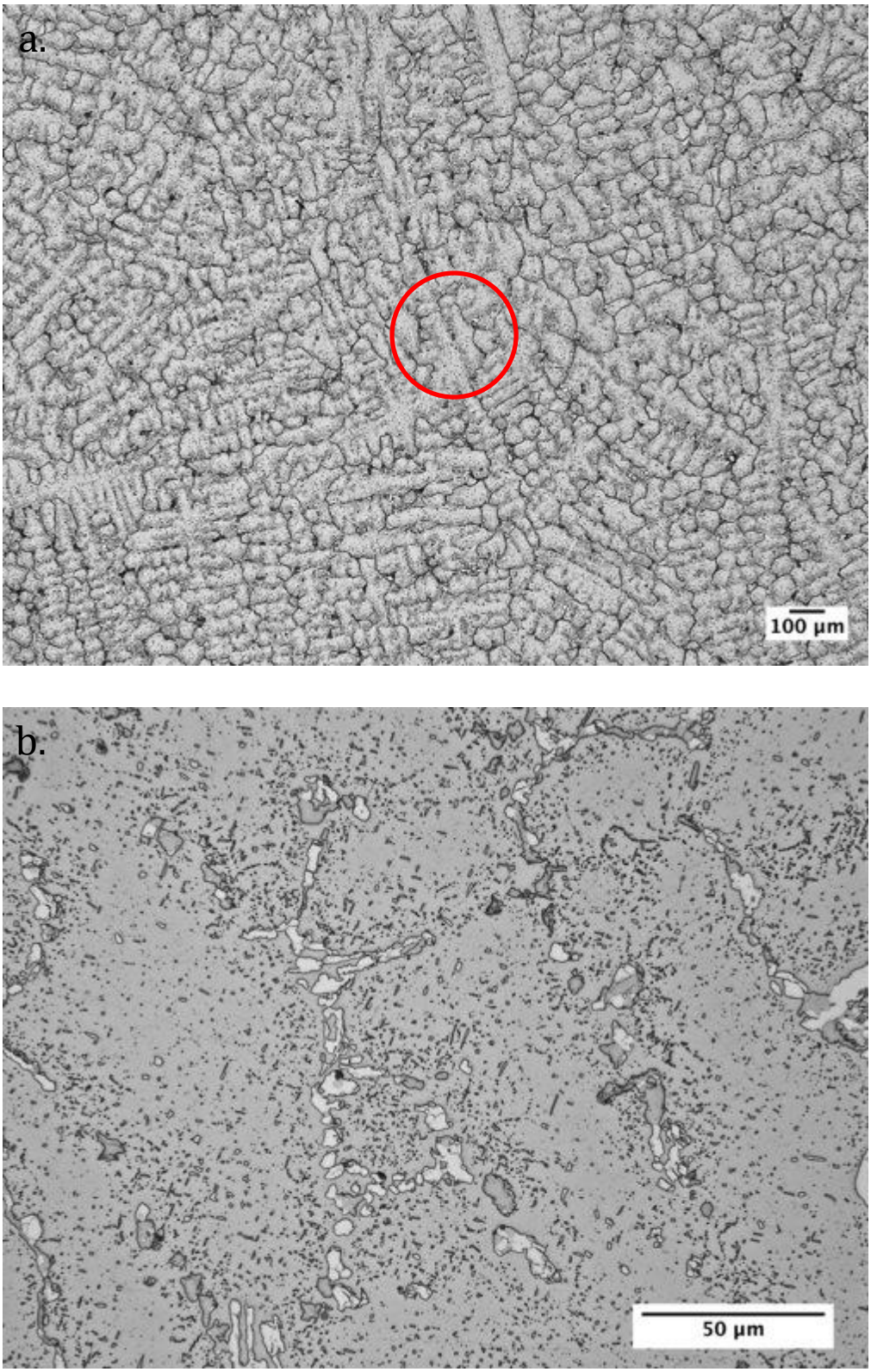

Figure 7. HP tube sample 3M2P2-SE OLM micrographs at a) 27.5X and b) 275X printed magnification.

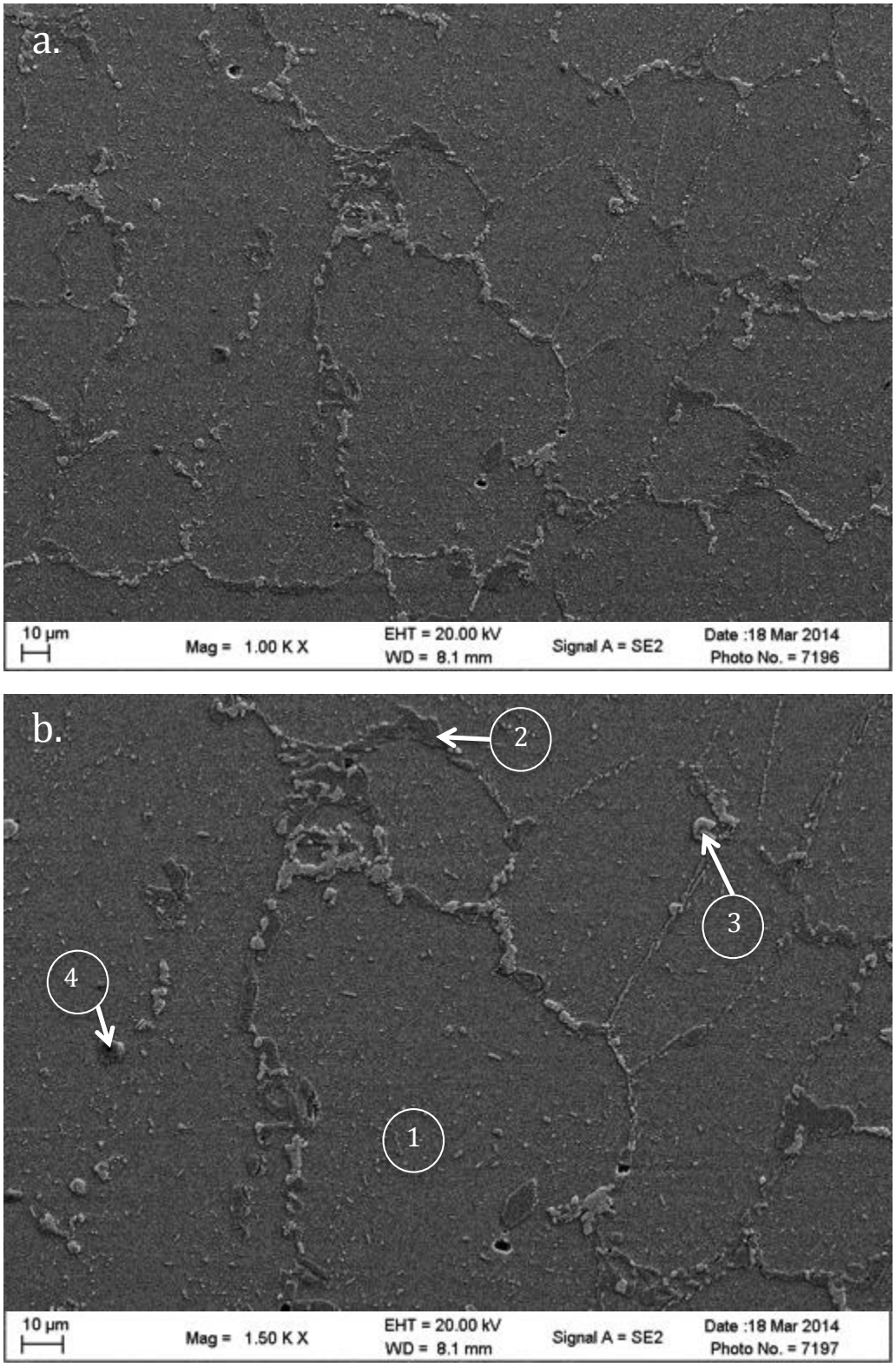

Figure 8. HP tube sample 3M2P2-SE SEM micrographs at a) 550X and b) 825X printed magnification. The marked areas in image b are examples of 1: the dendrite core region with secondary precipitates, 2: a type I carbide, 3: a type II carbide, and 4: a void.

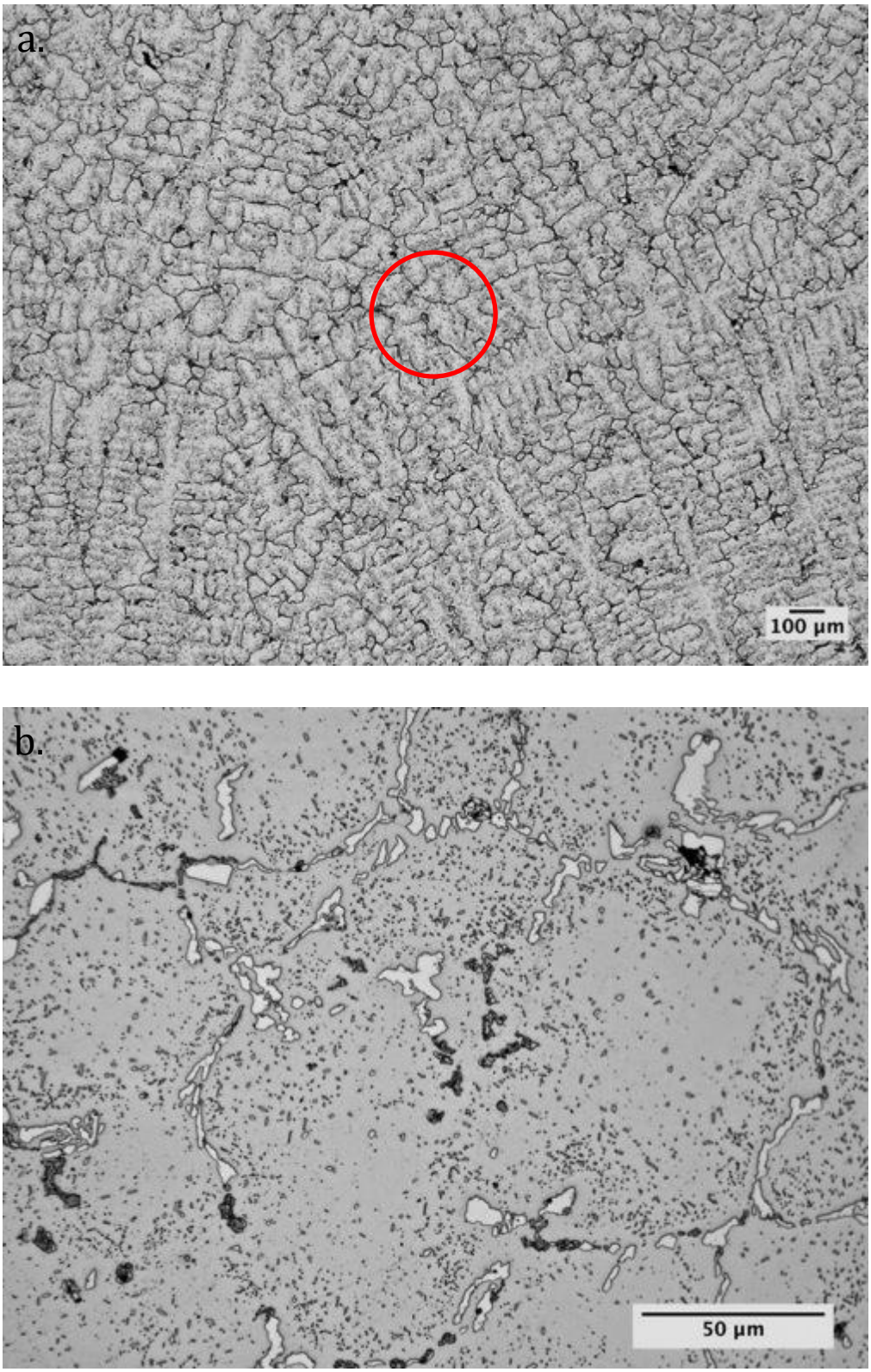

Figure 9. HP tube sample 3M2P2-CT[Ax] OLM micrographs at a) 27.5X and b) 275X printed magnification.

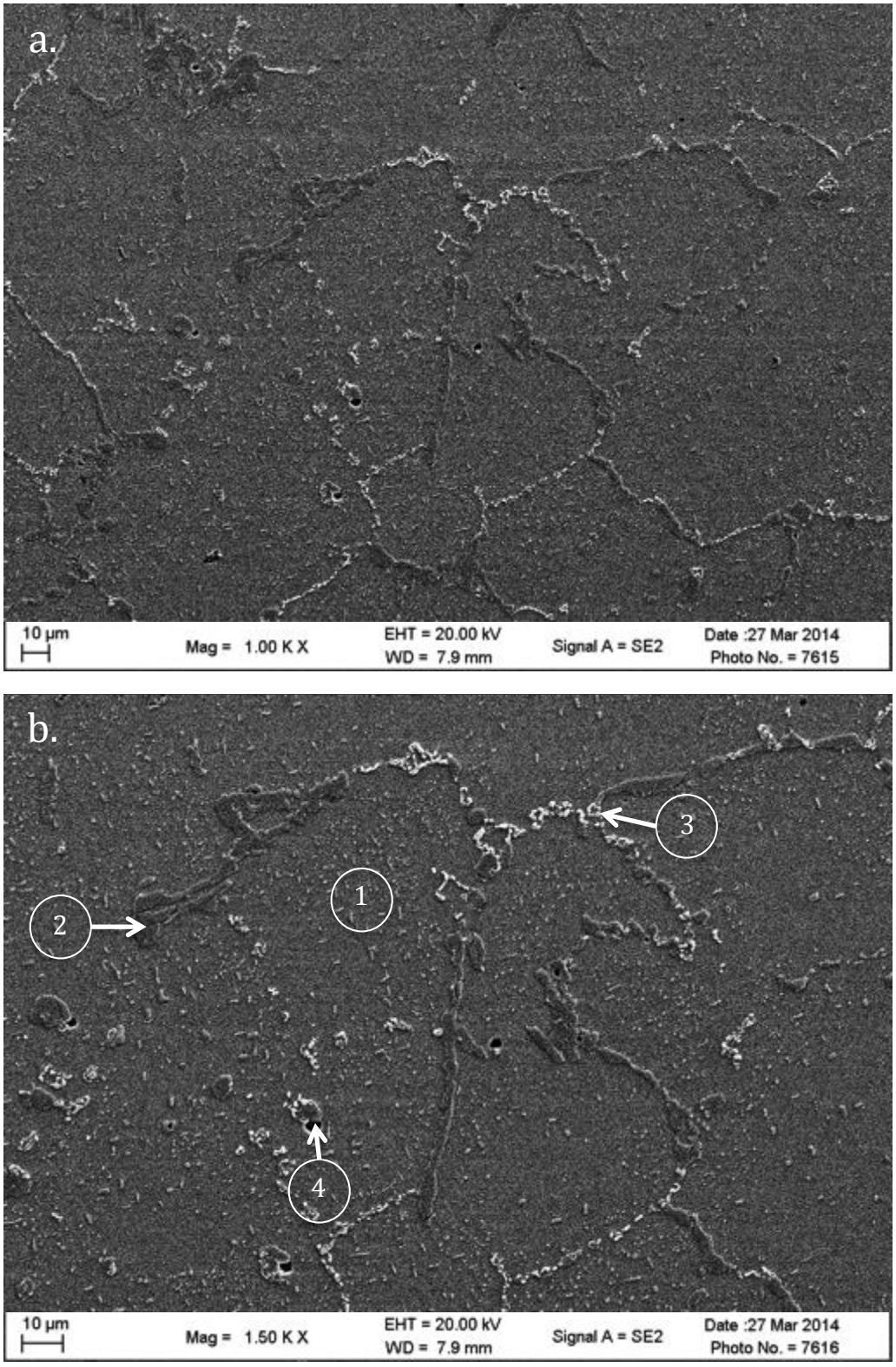

Figure 10. HP tube sample 3M2P2-CT[Ax] SEM micrographs at a) 550X and b) 825X printed magnification. The marked areas in image b are examples of 1: the dendrite core region with secondary precipitates, 2: a type I carbide, 3: a type II carbide, and 4: a void.

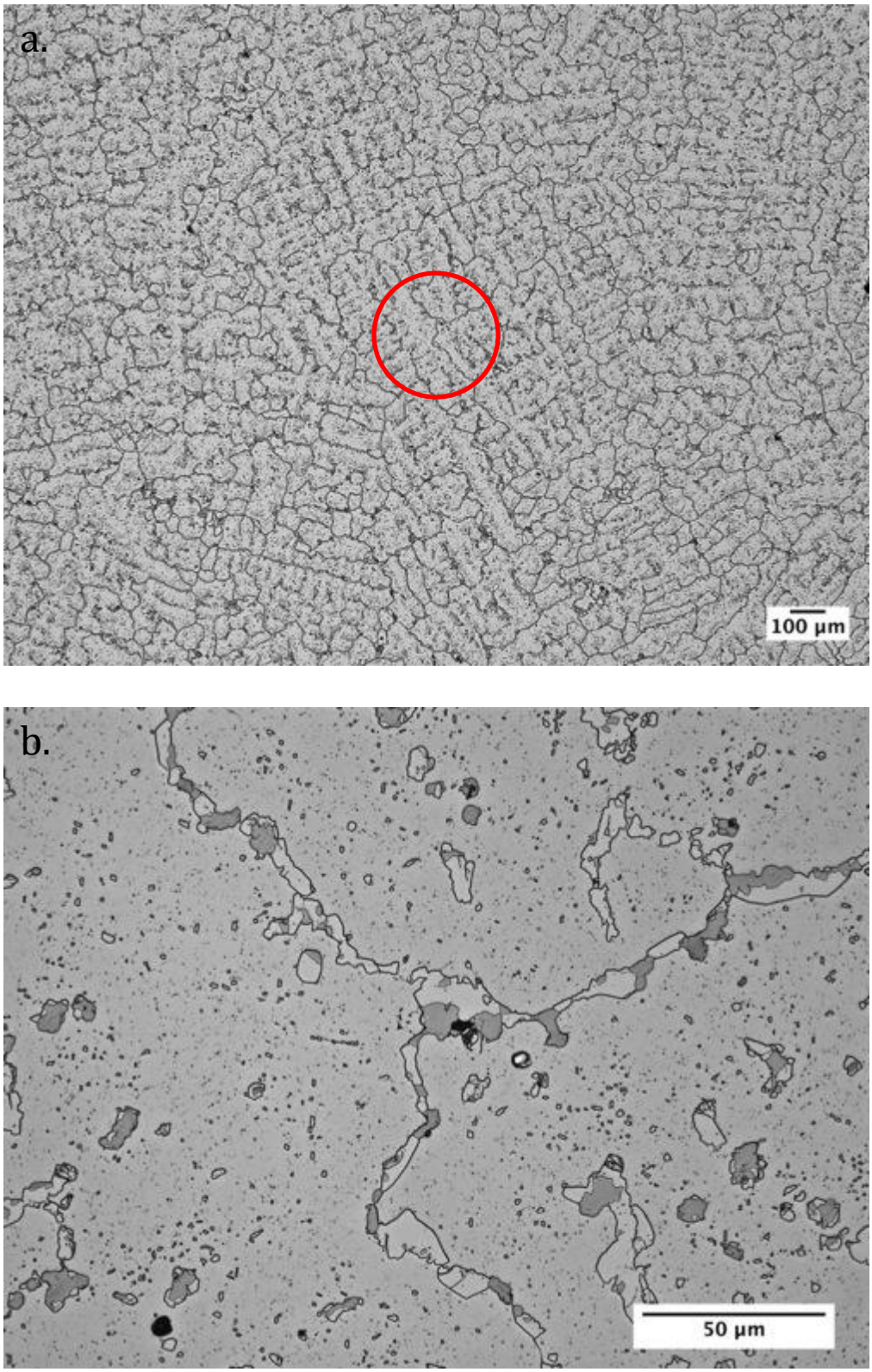

Figure 11. HP tube sample 4M3P3-SE OLM micrographs at a) 27.5X and b) 275X printed magnification.

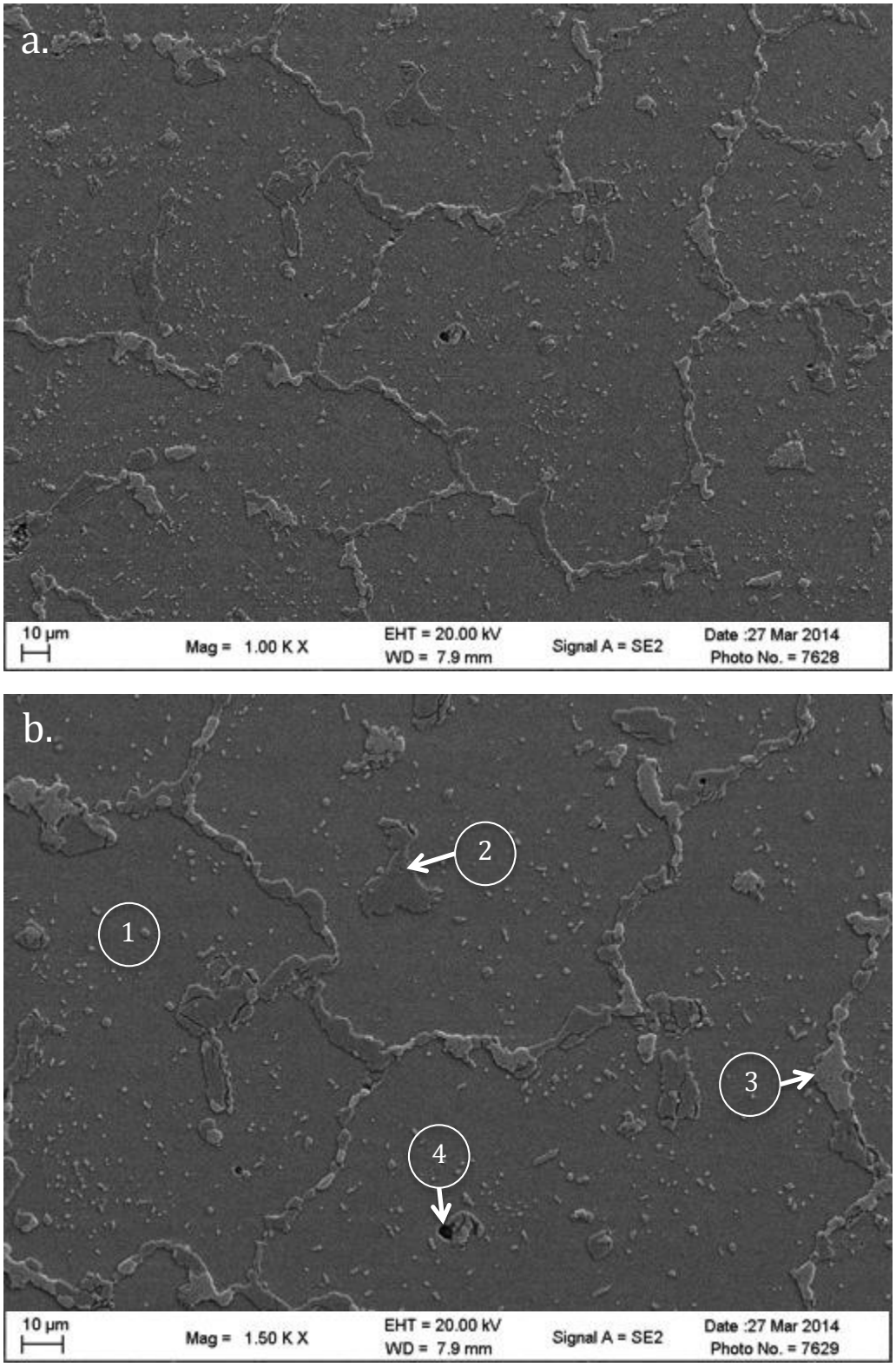

Figure 12. HP tube sample 4M3P3-SE SEM micrographs at a) 550X and b) 825X printed magnification. The marked areas in image b are examples of 1: the dendrite core region with secondary precipitates, 2: a type I carbide, 3: a type II carbide, and 4: a void.

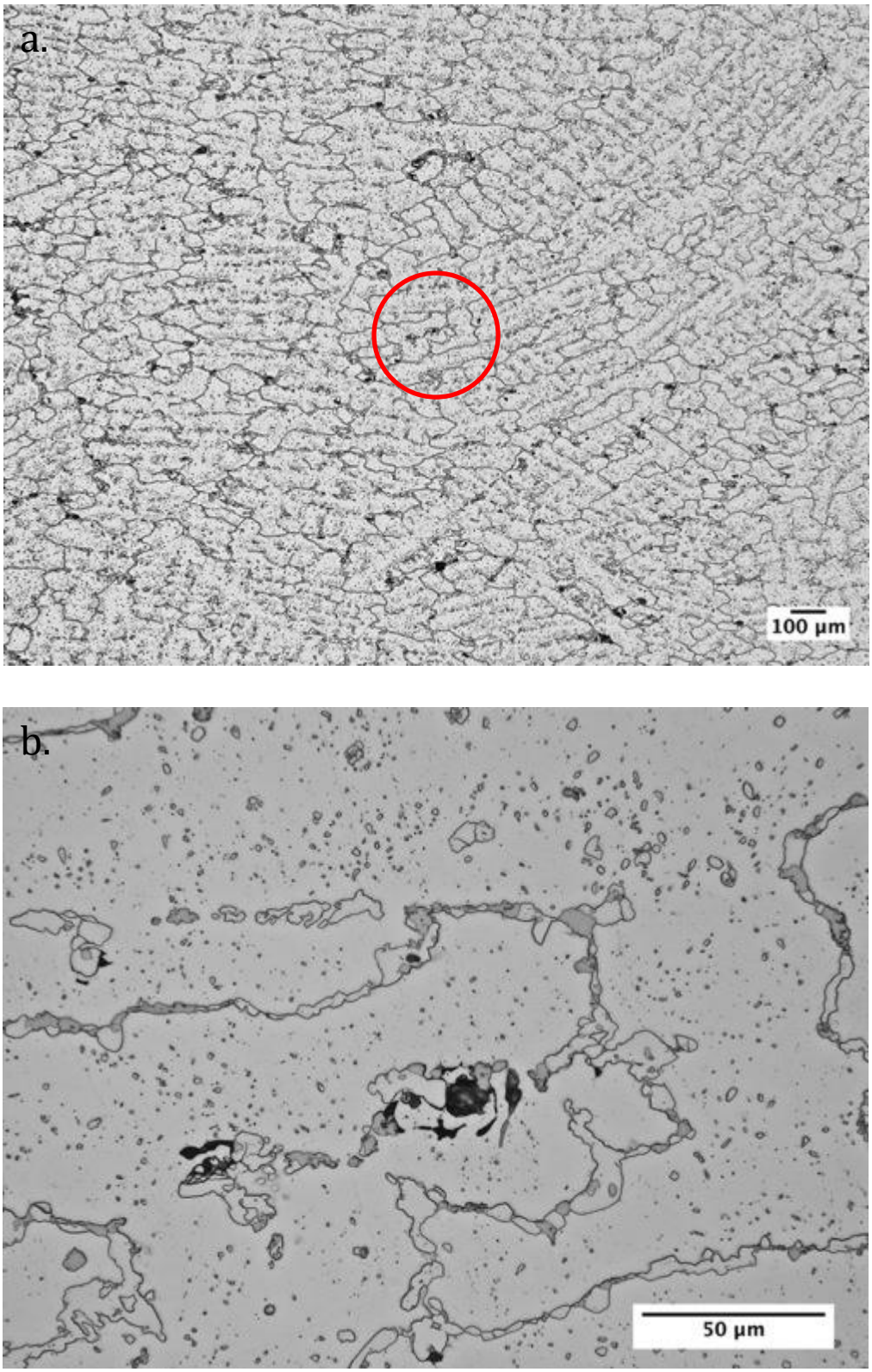

Figure 13. HP tube sample 4M3P3-CT[Ax] OLM micrographs at a) 27.5X and b) 275X printed magnification.

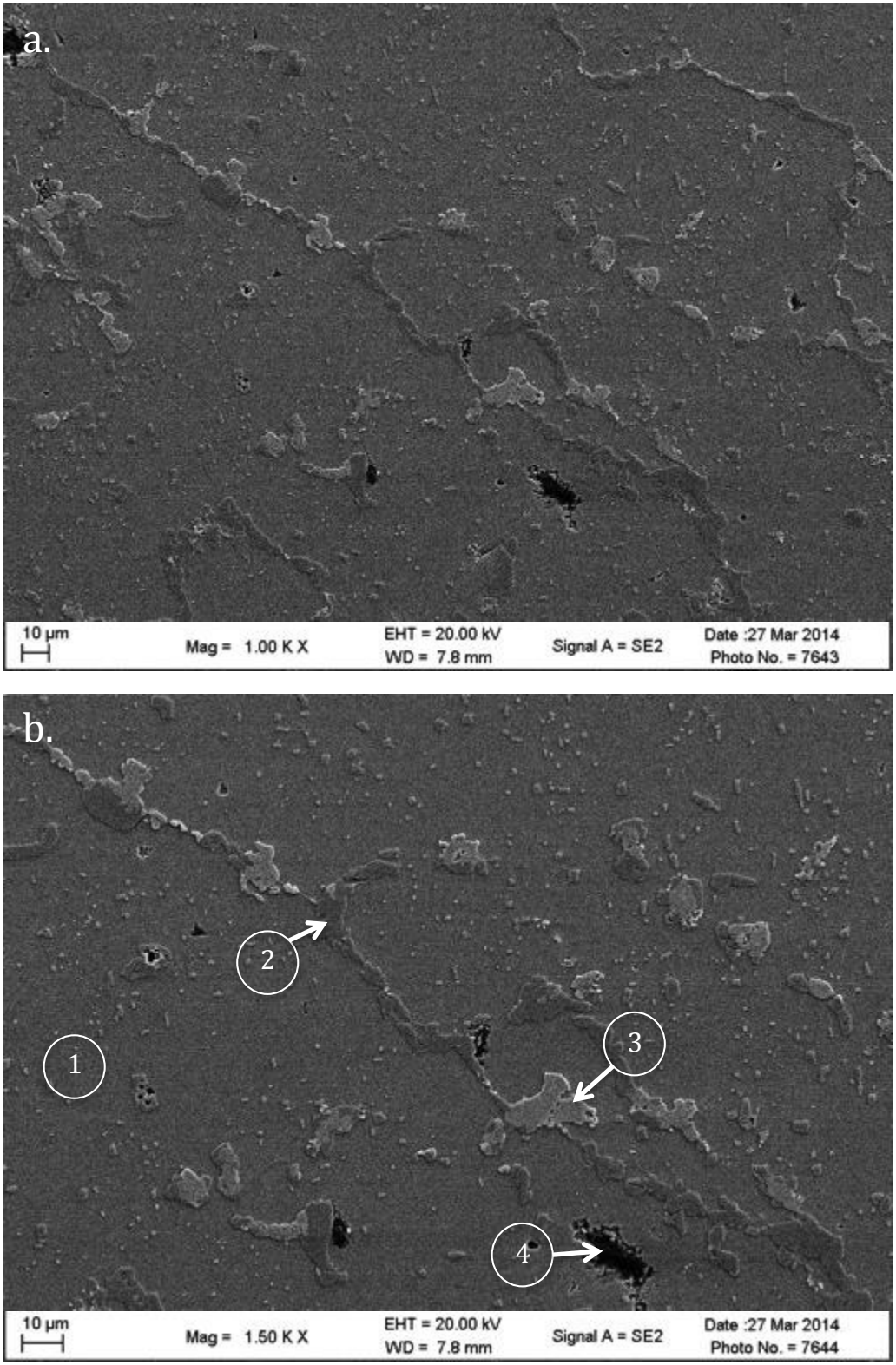

Figure 14. HP tube sample 4M3P3-CT[Ax] SEM micrographs at a) 550X and b) 825X printed magnification. The marked areas in image b are examples of 1: the dendrite core region with secondary precipitates, 2: a type I carbide, 3: a type II carbide, and 4: a void.

Table 5. Analysis of element composition of microstructural features of service exposed and creep tested samples of tube sample 1M1P1 from EDS analysis. The labels of the dendrite core regions, type I carbides and type II carbides are taken from the marked SEM images in Figures 4 and 6.

Sample	1M1P1-SE			1M1P1-CT[Ax]		
Detected Elements (wt%)	Dendrite Core Region (1)	Carbide Type I (2)	Carbide Type II (3)	Dendrite Core Region (1)	Carbide Type I (2)	Carbide Type II (3)
Cr	20	70	42	21	83	35
Fe	39	13	12	41	11	9
Ni	38	9	9	38	6	8

Table 6. Analysis of element composition of microstructural features of service exposed and creep tested samples of tube sample 3M2P2 from EDS analysis. The labels of the dendrite core regions, type I carbides and type II carbides are taken from the marked SEM images in Figures 8 and 10.

Sample	3M2P2-SE			3M2P2-CT[Ax]		
Detected Elements (wt%)	Dendrite Core Region (1)	Carbide Type I (2)	Carbide Type II (3)	Dendrite Core Region (1)	Carbide Type I (2)	Carbide Type II (3)
Cr	23	79	8	23	79	11
Fe	37	8	10	35	7	14
Ni	38	5	46	35	4	13
Nb			21			58

Table 7. Analysis of element composition of microstructural features of service-exposed and creep-tested samples of tube sample 4M3P3 from EDS analysis. The labels of the dendrite core regions, type I carbides and type II carbides are taken from the marked SEM images in Figures 12 and 14.

Sample	4M3P3-SE			4M3P3-CT[Ax]		
Detected Elements (wt%)	Dendrite Core Region (1)	Carbide Type I (2)	Carbide Type II (3)	Dendrite Core Region (1)	Carbide Type I (2)	Carbide Type II (3)
Cr	22	74	2	21	76	8
Fe	38	9	5	41	7	8
Ni	35		48	32	4	6
Nb			33			77

6.4: Void Comparison

Figures 15 through 22 list the void count results for the service exposed and post-creep test samples. The void counts of the creep tested samples were extracted along the center of the gauge length perpendicular to the tube wall and compared to the service exposed sample in the same orientation. This was done in order to achieve the best possible comparison of volume percent voids before and after creep testing to evaluate their formation. The axial creep test samples (CT[Ax]) are compared to the longitudinal ex-service samples and the circumferential creep test samples (CT[Circ1 or 2]) are compared to the transverse ex-service samples.

As evidenced in Figures 15-22, the relationship between the service exposed samples and the creep tested samples varies greatly between the HP alloy tubes. While the general trend is for the creep tested samples to have a greater calculated volume percentage of voids with no significant difference between creep testing directions, samples 1M1P1-CT[Circ1], 3M2P2-CT[Ax], 3M2P2-CT[Circ2], 4M3P3-CT[Ax], 5M3P3-CT[Ax], 5M3P3-CT[Circ1], 6M3P4-CT[Circ1], 7M3P4-CT[Ax], 7M3P4-CT[Circ1], 8M3P5-CT[Ax], and 8M3P5-CT[Circ1] all have at least one service exposed measurement greater than the corresponding creep measurement. This indicates that there is quite a bit of void variation along the length of the tube since the creep test samples were removed from different sections of the tube than the ring samples used for the service exposed analysis. For both the service exposed and creep tested samples, the greatest volume percentage of voids most often occurs inside either the inside or outside diameter locations with the lowest amount of void growth usually occurring in the center of thickness. This is more than likely due to the damaging effects of the environment in which the reformer tubes operate but may also be an indicator of the presence of fine grains within the tube wall. Comparing the calculated volume percent voids between tubes, it can be shown that overall the tubes from manufacturers M1 and M2 experienced lesser amounts of void formation during service than the tubes from manufacturer M3.

Samples 2M1P1-CT[Circ1] and 3M2P2-CT[Circ1], in Figures 16 and 17 respectively, both ruptured during the creep test. The rupture these samples experienced is indicated by the large increase in volume percent voids from the service exposed condition in comparison to the other creep tests performed on the same tube sample. This

void volume percent expansion indicates that most of the void growth occurs in the last 5% of life. In addition, both samples had the greatest volume percent of voids adjacent to the inside diameter and at the center of thickness, indicating the presence of fine grains at these locations (shown in Figures 24 and 25).

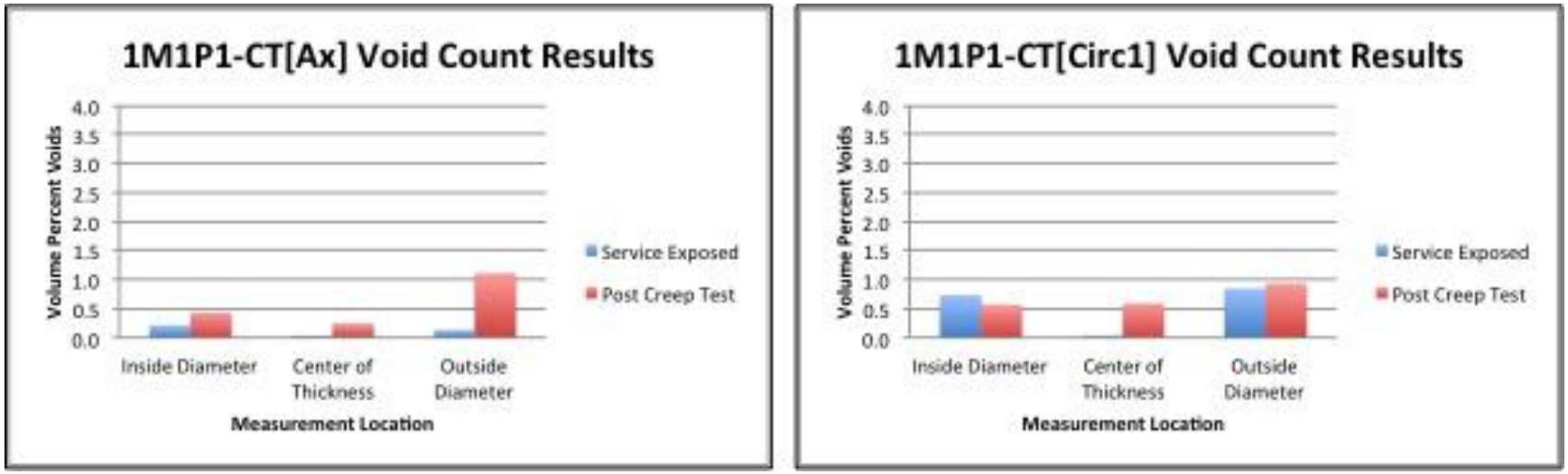

Figure 15. Void count results for the creep samples from the ex-service HP tube 1M1P1 compared to the service-exposed sample of the same orientation. Measurements were taken at areas of the samples corresponding to just inside the inside diameter, the center of thickness, and just inside the outside diameter of the tube. The axially tested creep sample is compared to the longitudinal ex-service sample and the circumferentially creep tested sample is compared to the transverse ex-service sample.

Figure 16. Void count results for the creep samples from the ex-service HP tube 2M1P1 compared to the service-exposed sample of the same orientation. Measurements were taken from areas of the samples corresponding to just inside the inside diameter, the center of thickness, and just inside the outside diameter of the tube. The axially tested creep sample is compared to the longitudinal ex-service sample and the circumferentially creep tested sample is compared to the transverse ex-service sample. Sample B20-CT[Circ1] ruptured before the test could be interrupted.

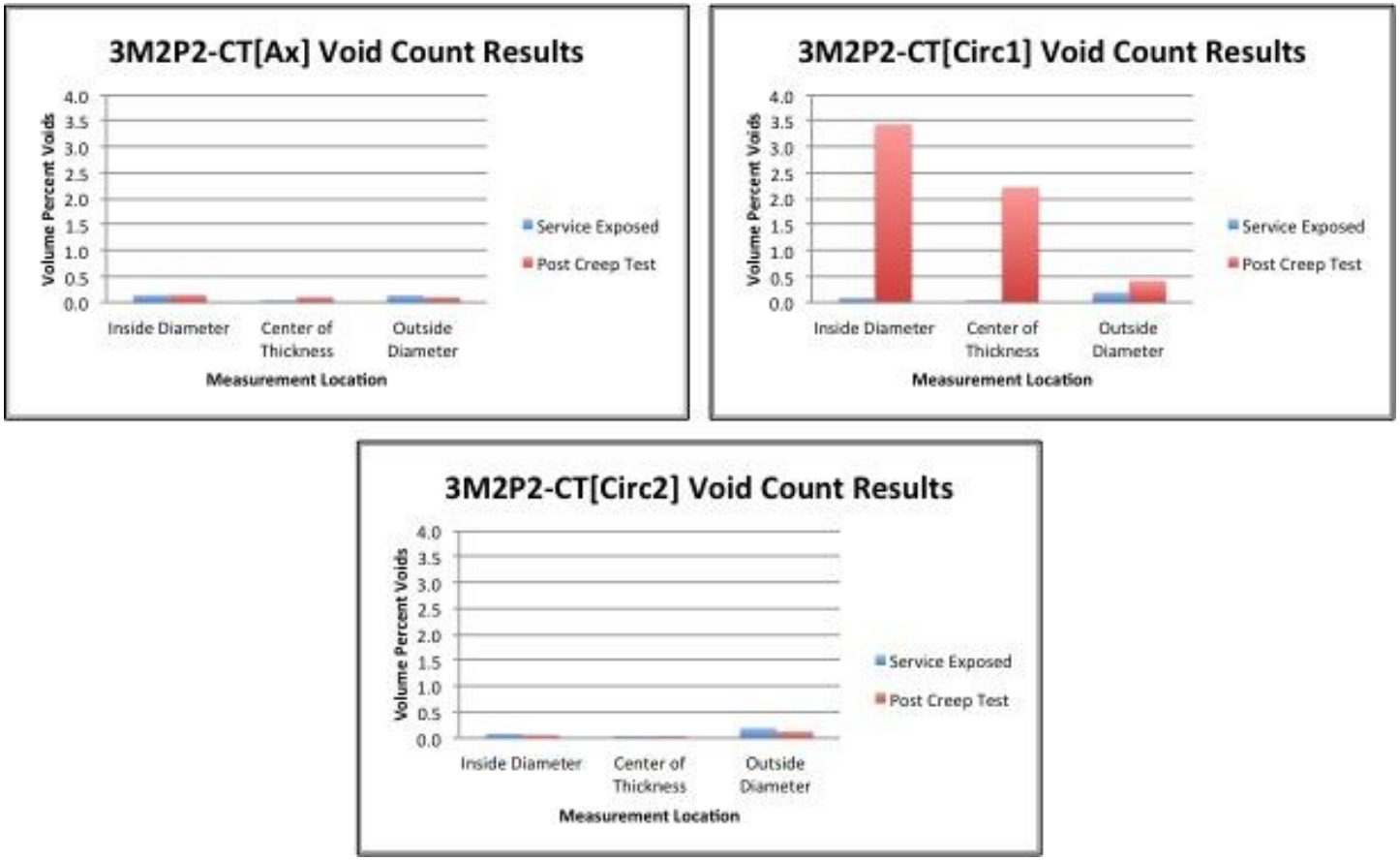

Figure 17. Void count results for the creep samples from the ex-service HP tube 3M2P2 compared to the service-exposed sample of the same orientation. Measurements were taken from areas of the samples corresponding to just inside the inside diameter, the center of thickness, and just inside the outside diameter of the tube. The axially tested creep sample is compared to the longitudinal ex-service sample and the circumferentially creep tested sample is compared to the transverse ex-service sample. Sample R2T27-CT[Circ1] ruptured before the test could be interrupted.

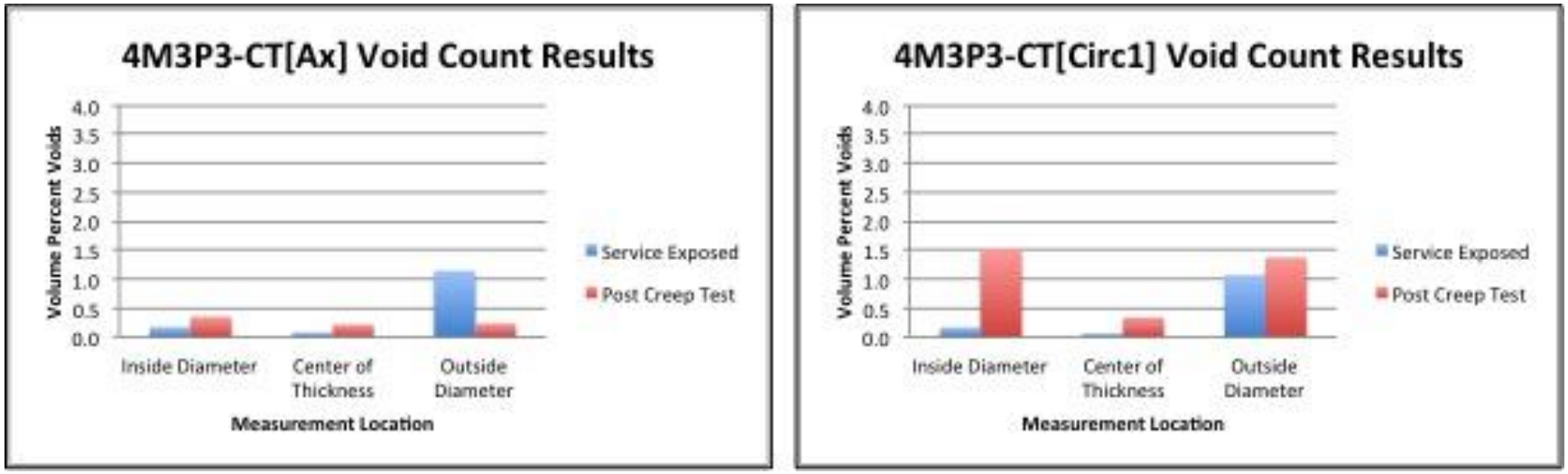

Figure 18. Void count results for the creep samples from the ex-service HP tube 4M3P3 compared to the service-exposed sample of the same orientation. Measurements were taken from areas of the samples corresponding to just inside the inside diameter, the center of thickness, and just inside the outside diameter of the tube. The axially tested creep sample is compared to the longitudinal ex-service sample and the circumferentially creep tested sample is compared to the transverse ex-service sample.

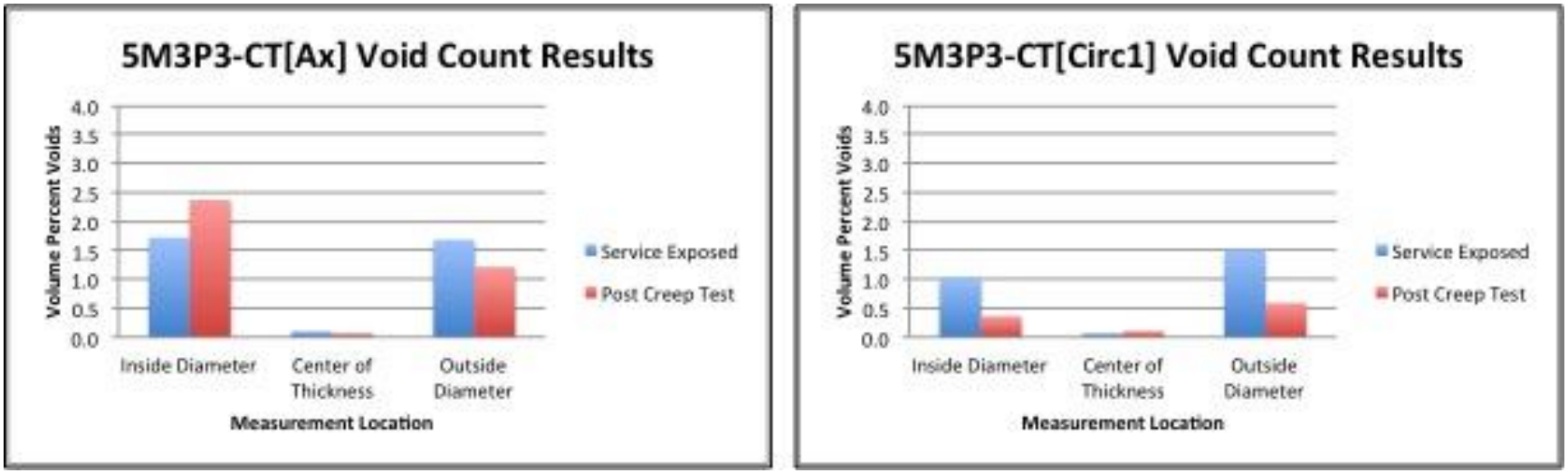

Figure 19. Void count results for the creep samples from the ex-service HP tube 5M3P3 compared to the service-exposed sample of the same orientation. Measurements were taken from areas of the samples corresponding to just inside the inside diameter, the center of thickness, and just inside the outside diameter of the tube. The axially tested creep sample is compared to the longitudinal ex-service sample and the circumferentially creep tested sample is compared to the transverse ex-service sample.

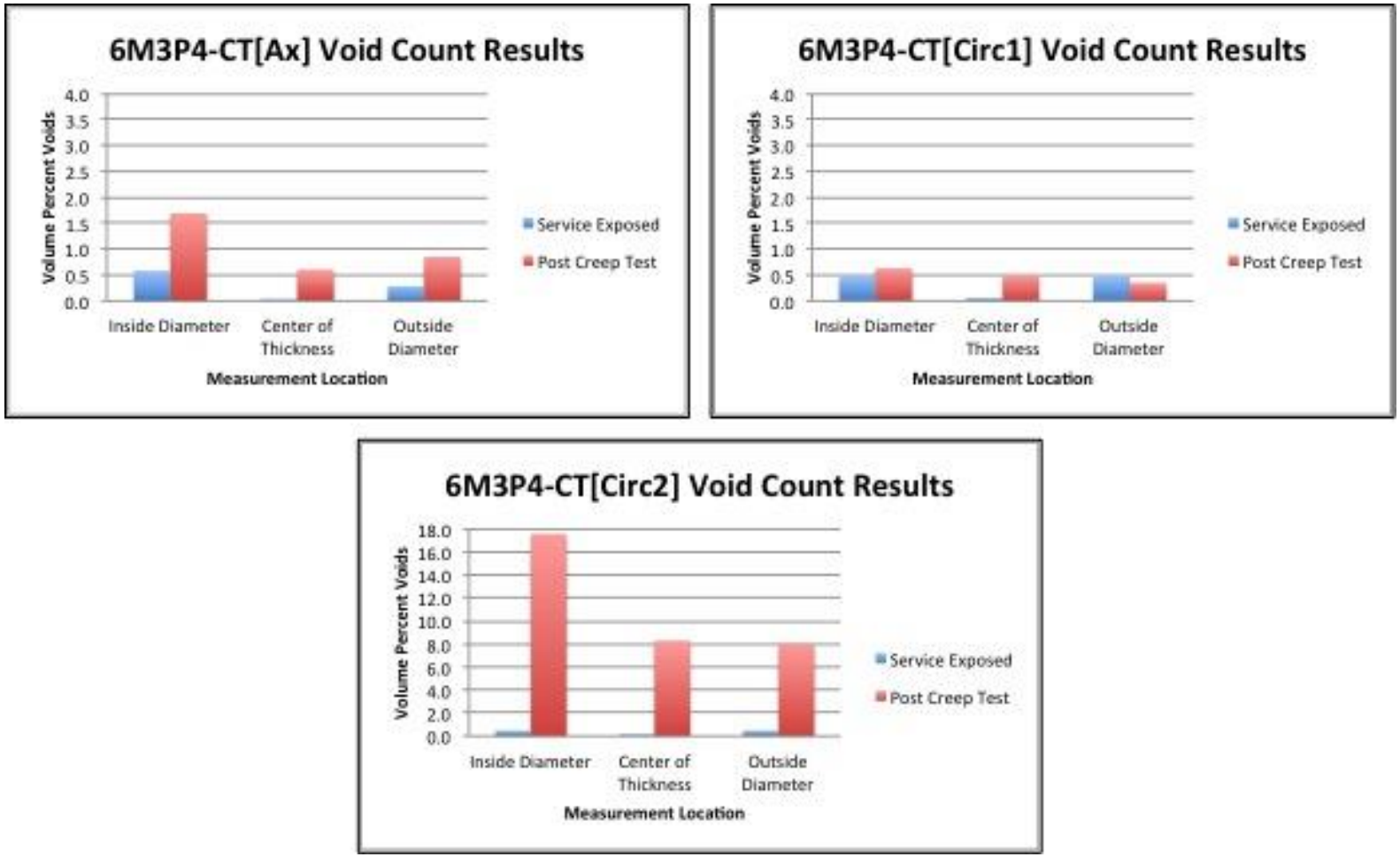

Figure 20. Void count results for the creep samples from the ex-service HP tube 6M3P4 compared to the service-exposed sample of the same orientation. Measurements were taken from areas of the samples corresponding to just inside the inside diameter, the center of thickness, and just inside the outside diameter of the tube. The axially tested creep sample is compared to the longitudinal ex-service sample and the circumferentially creep tested sample is compared to the transverse ex-service sample.

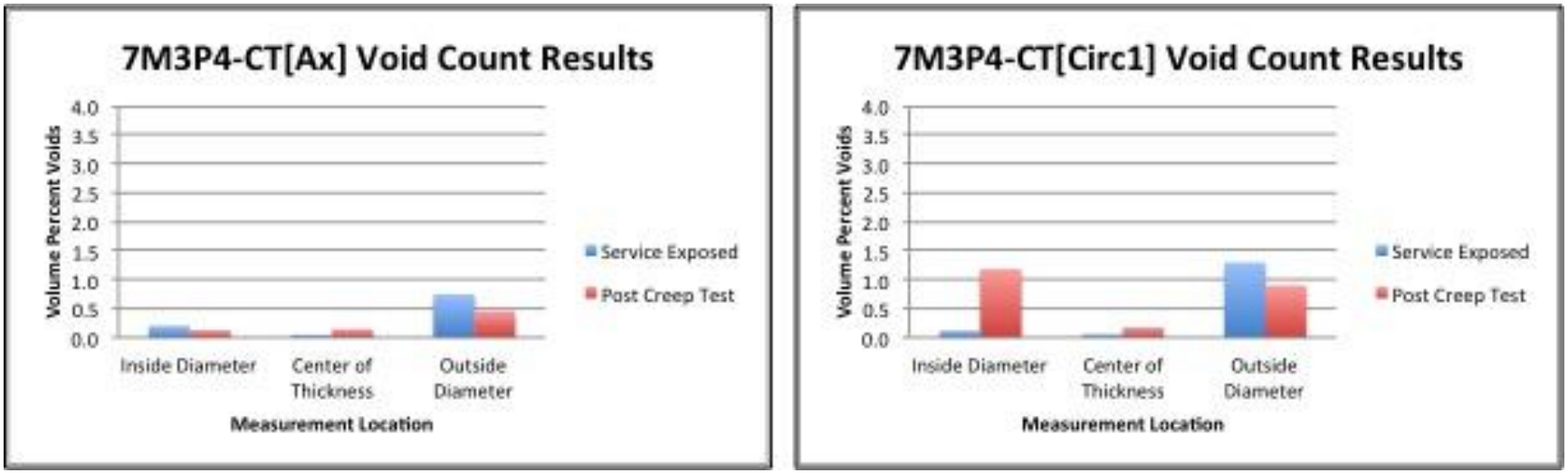

Figure 21. Void count results for the creep samples from the ex-service HP tube 7M3P4 compared to the service-exposed sample of the same orientation. Measurements were taken from areas of the samples corresponding to just inside the inside diameter, the center of thickness, and just inside the outside diameter of the tube. The axially tested creep sample is compared to the longitudinal ex-service sample and the circumferentially creep tested sample is compared to the transverse ex-service sample.

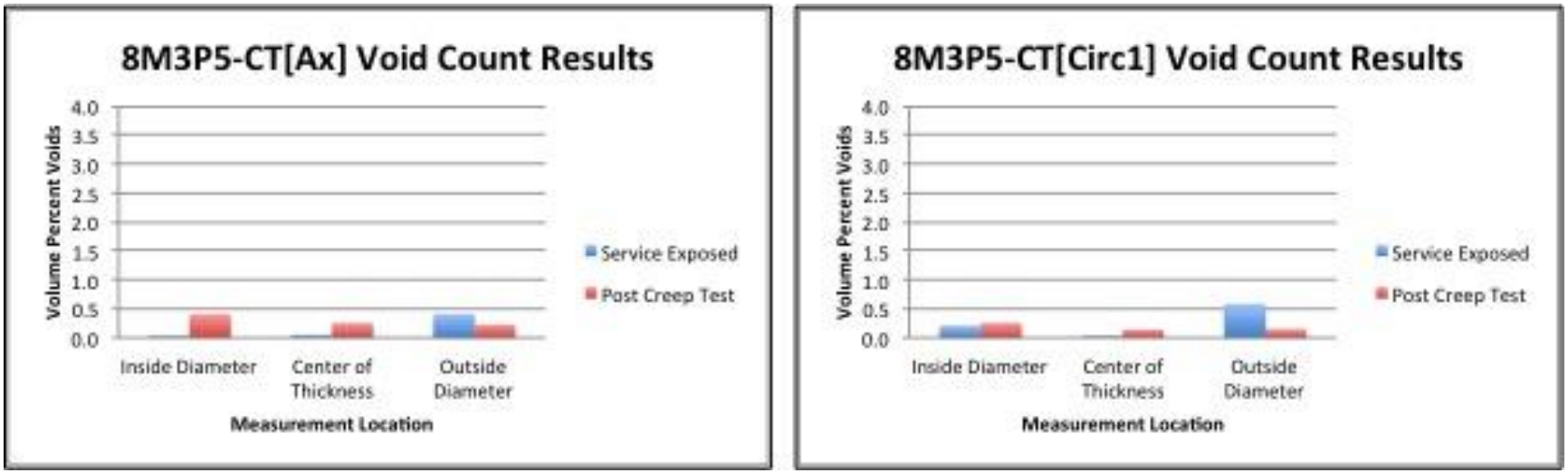

Figure 22. Void count results for the creep samples from the ex-service HP tube 8M3P5 compared to the service-exposed sample of the same orientation. Measurements were taken from areas of the samples corresponding to just inside the inside diameter, the center of thickness, and just inside the outside diameter of the tube. The axially tested creep sample is compared to the longitudinal ex-service sample and the circumferentially creep tested sample is compared to the transverse ex-service sample.

6.5: Macrostructure

Photo macrographs of the macrostructure of the ex-service samples were taken in order to identify the arrangement and structure of the grains within the tubes as well as to determine the ratio of fine grains to elongated columnar grains in the tube wall. All of the imaging was successfully completed and then analyzed using the procedures outlined in Section 4.6. The following results include an observational analysis of the optical images as well as results from the analyses to calculate the percent of fine grain in the sample walls.

6.5.1: Photo Macrographs

The photo macrographs of both the longitudinal and transverse of the ex-service tube ring samples are provided in Figures 23-30. As is shown in these macrographs, the grain composition of the tubes runs from completely composed of columnar grains (Figure 23, HP tube sample 1M1P1) to being nearly entirely composed of equiaxed fine grains (Figure 26, HP tube sample 4M3P3). It is important to note that the formation of fine grains within the walls of the analyzed tube samples is not restricted to one certain region. While the majority of the fine grain formation occurs against the inside diameter of the tube samples, fine grain bands are also shown to appear within the wall of the tube (see Figure 28, HP tube sample 6M3P4) and in thin bands at the outer diameter. The thin bands at the outer diameter are more than likely a result of rapid cooling of the molten metal as it touches the mold. Looking at the macrographs of the tube samples as a whole, it becomes apparent that neither manufacturer M1 or M3 has much control over the formation of grains in the samples. There is not enough information available to comment on the variability of manufacturer M2.

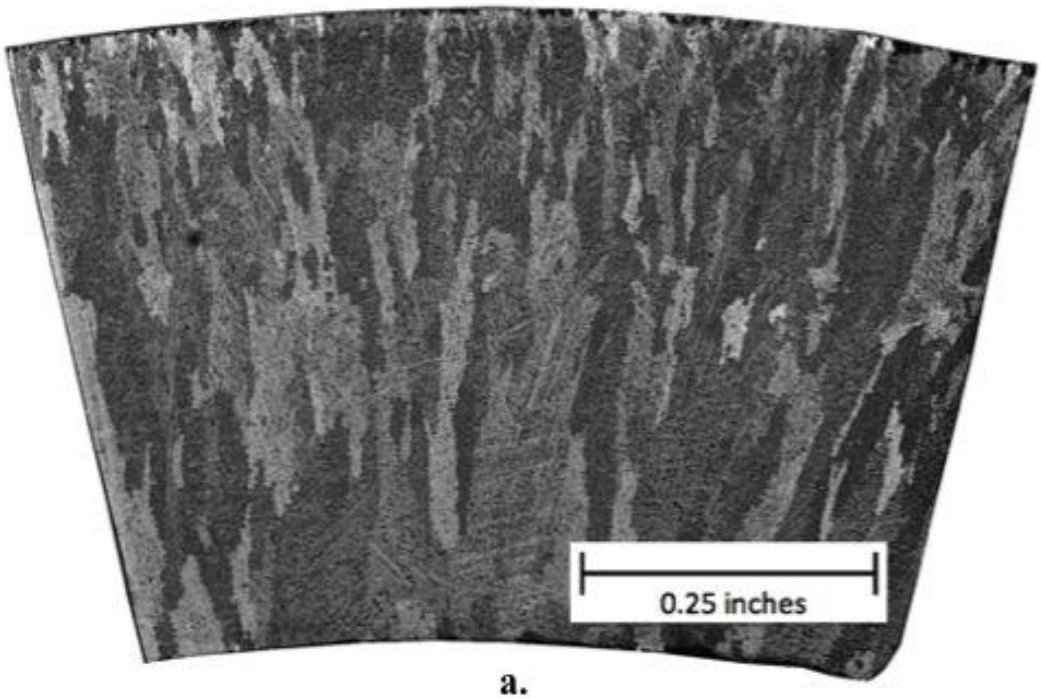

a.

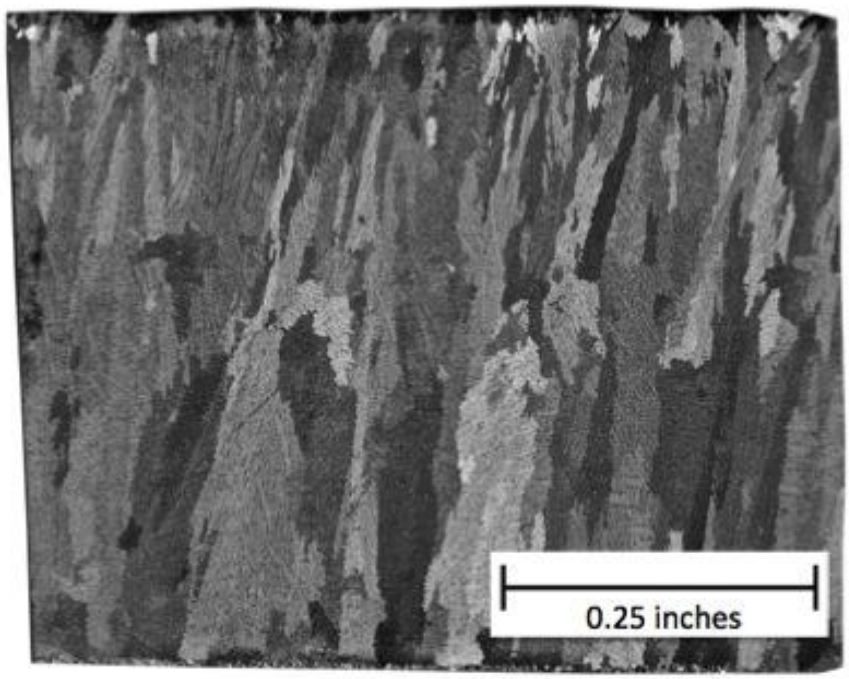

b.

Figure 23. Transverse (a) and longitudinal (b) photo macrographs of service exposed HP alloy tube sample 1M1P1.

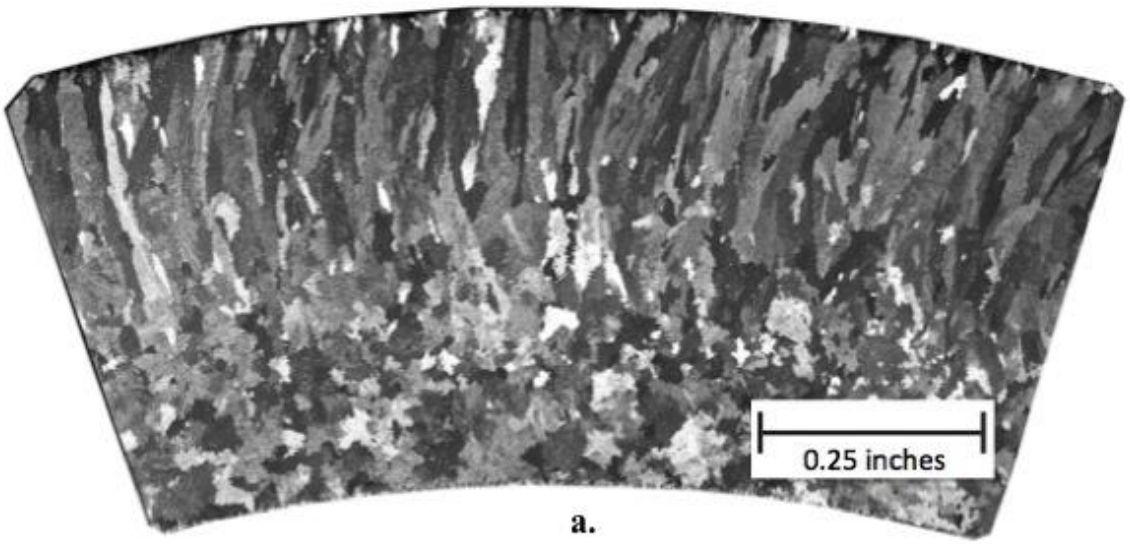

a.

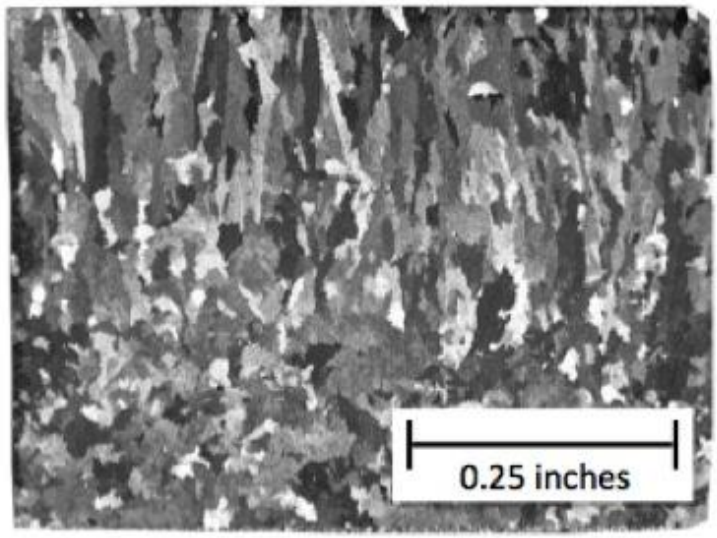

b.

Figure 24. Transverse (a) and longitudinal (b) photo macrographs of service exposed HP alloy tube sample 2M1P1.

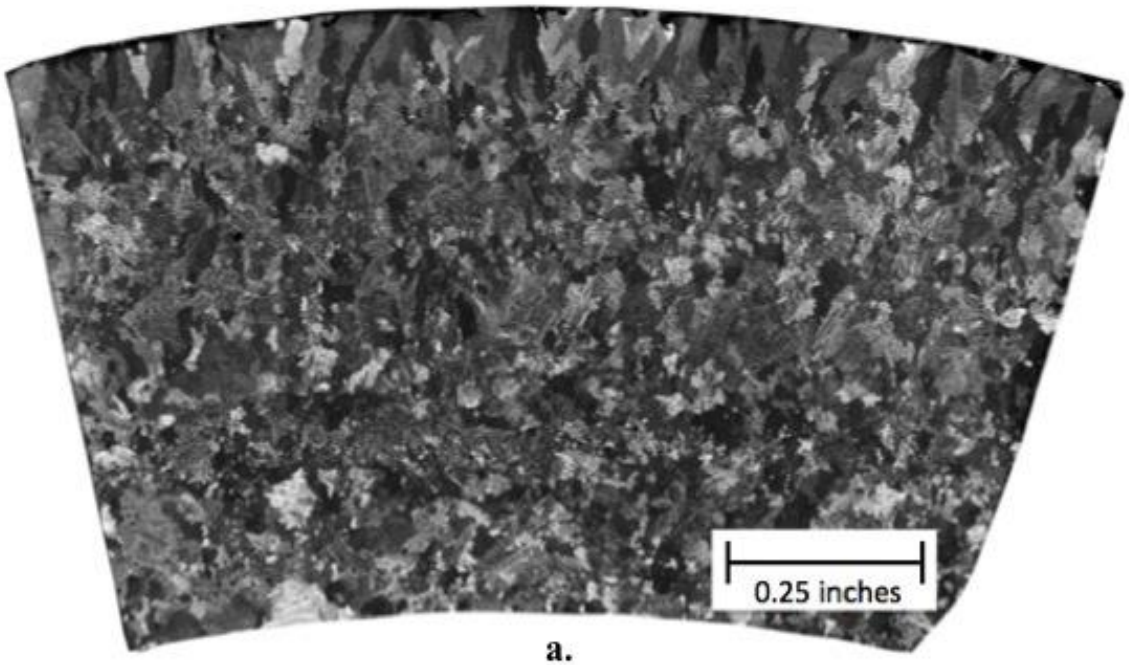

a.

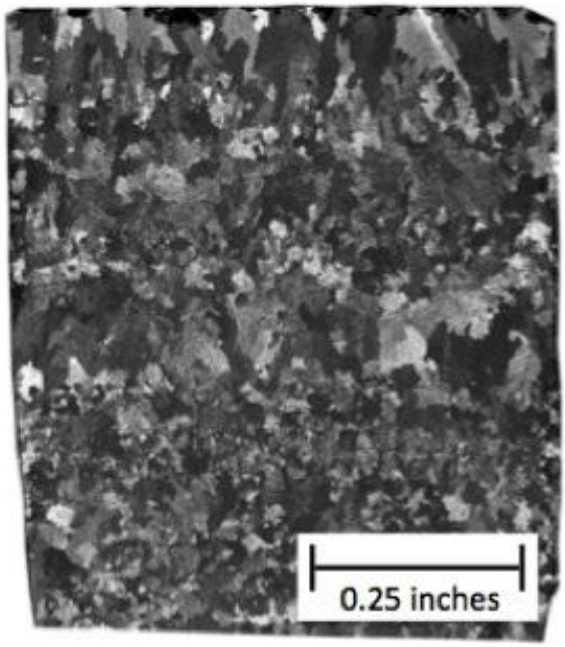

b.

Figure 25. Transverse (a) and longitudinal (b) photo macrographs of service exposed HP alloy tube sample 3M2P2.

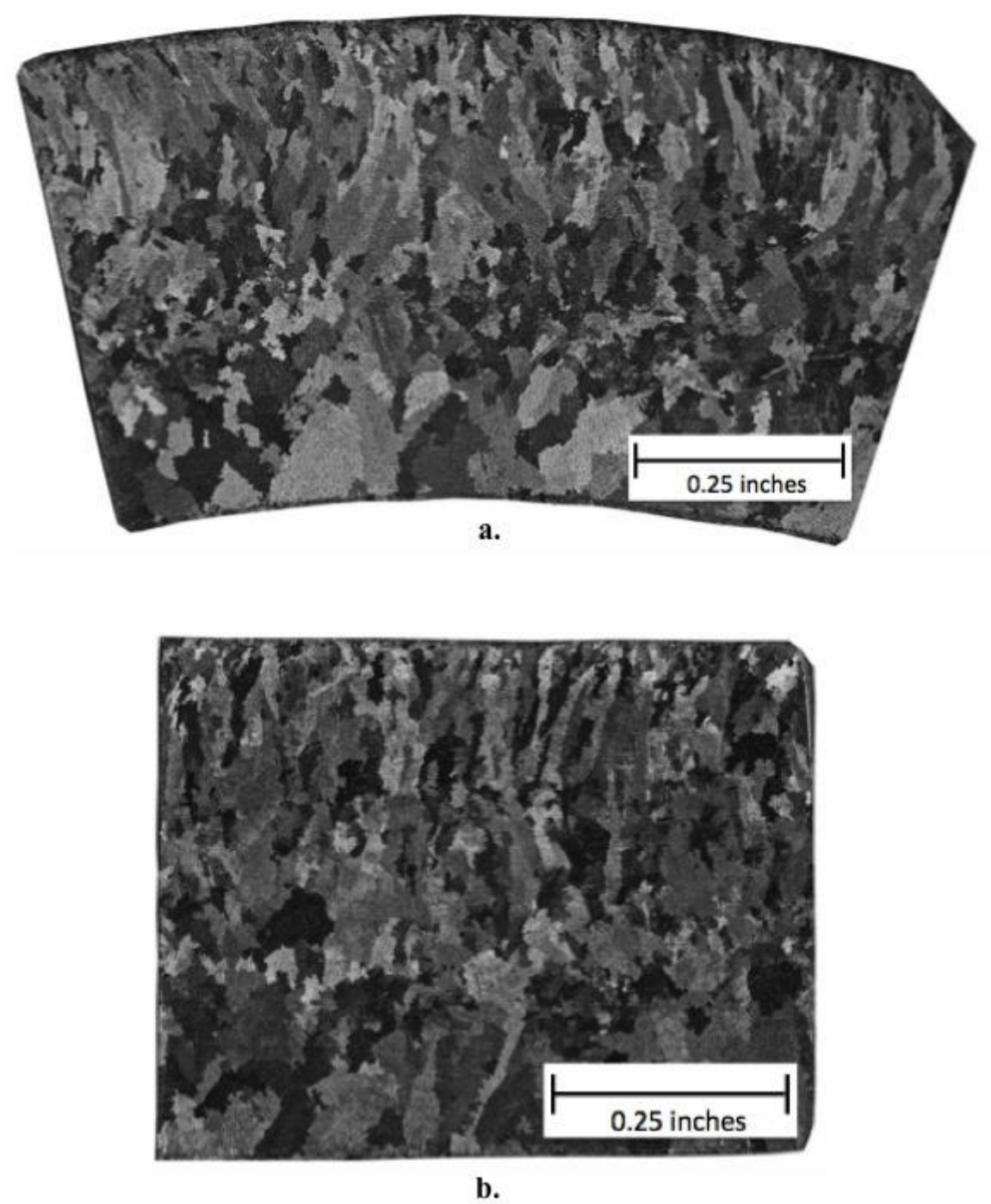

Figure 26. Transverse (a) and longitudinal (b) photo macrographs of service exposed HP alloy tube sample 4M3P3.

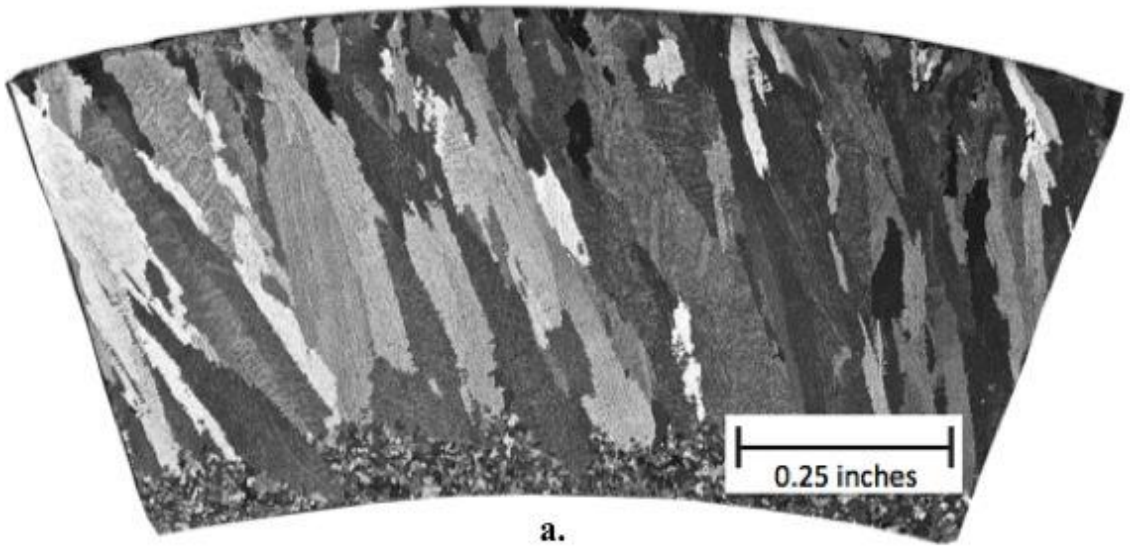

a.

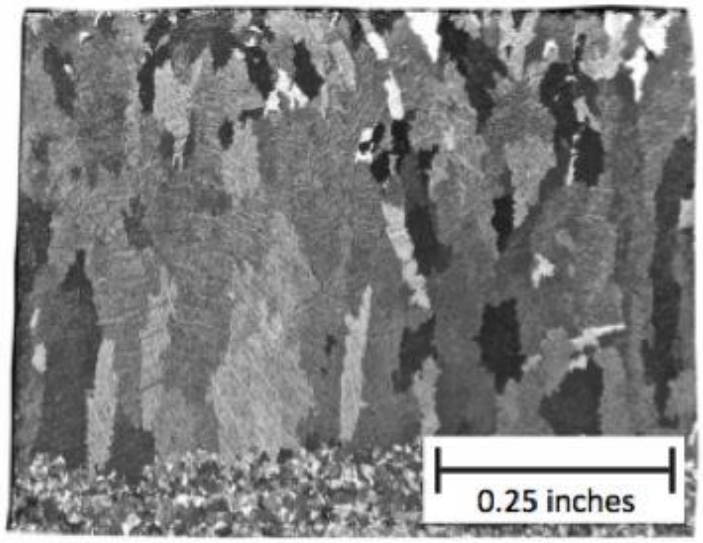

b.

Figure 27. Transverse (a) and longitudinal (b) photo macrographs of service exposed HP alloy tube sample 5M3P3.

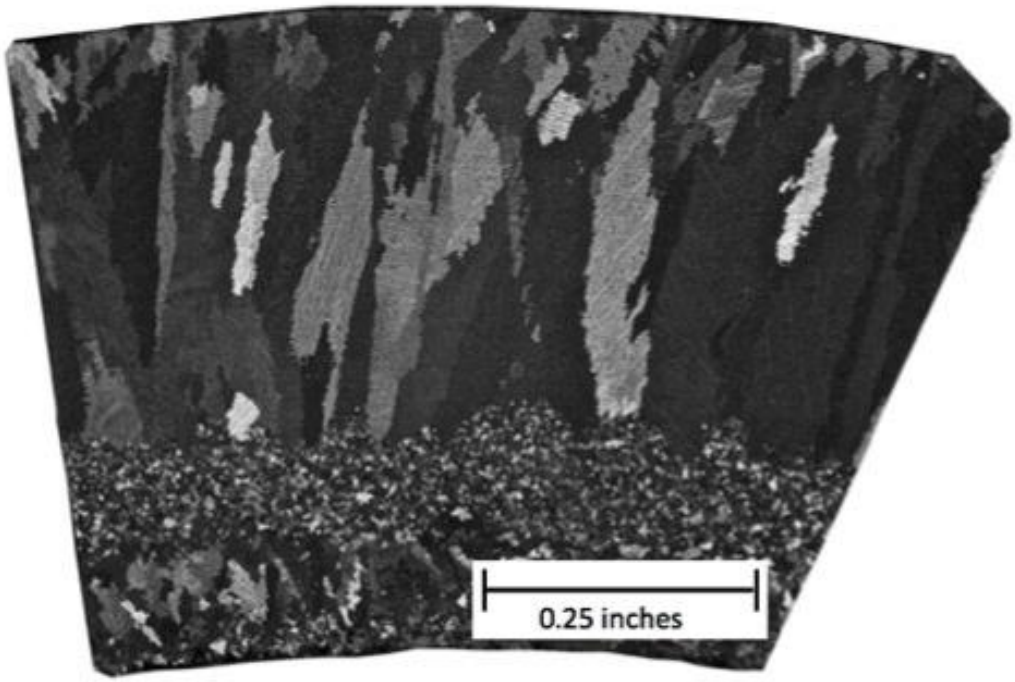

a.

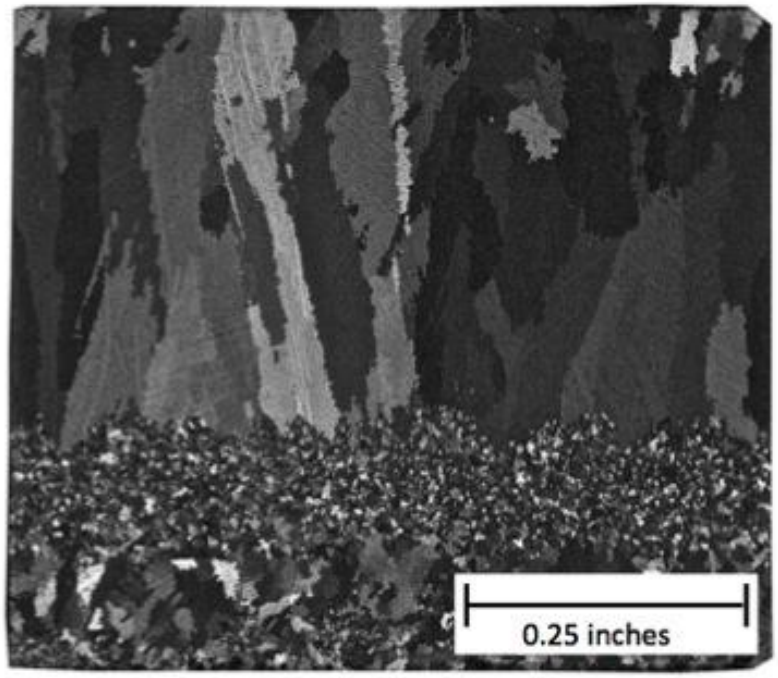

b.

Figure 28. Transverse (a) and longitudinal (b) photo macrographs of service exposed HP alloy tube sample 6M3P4.

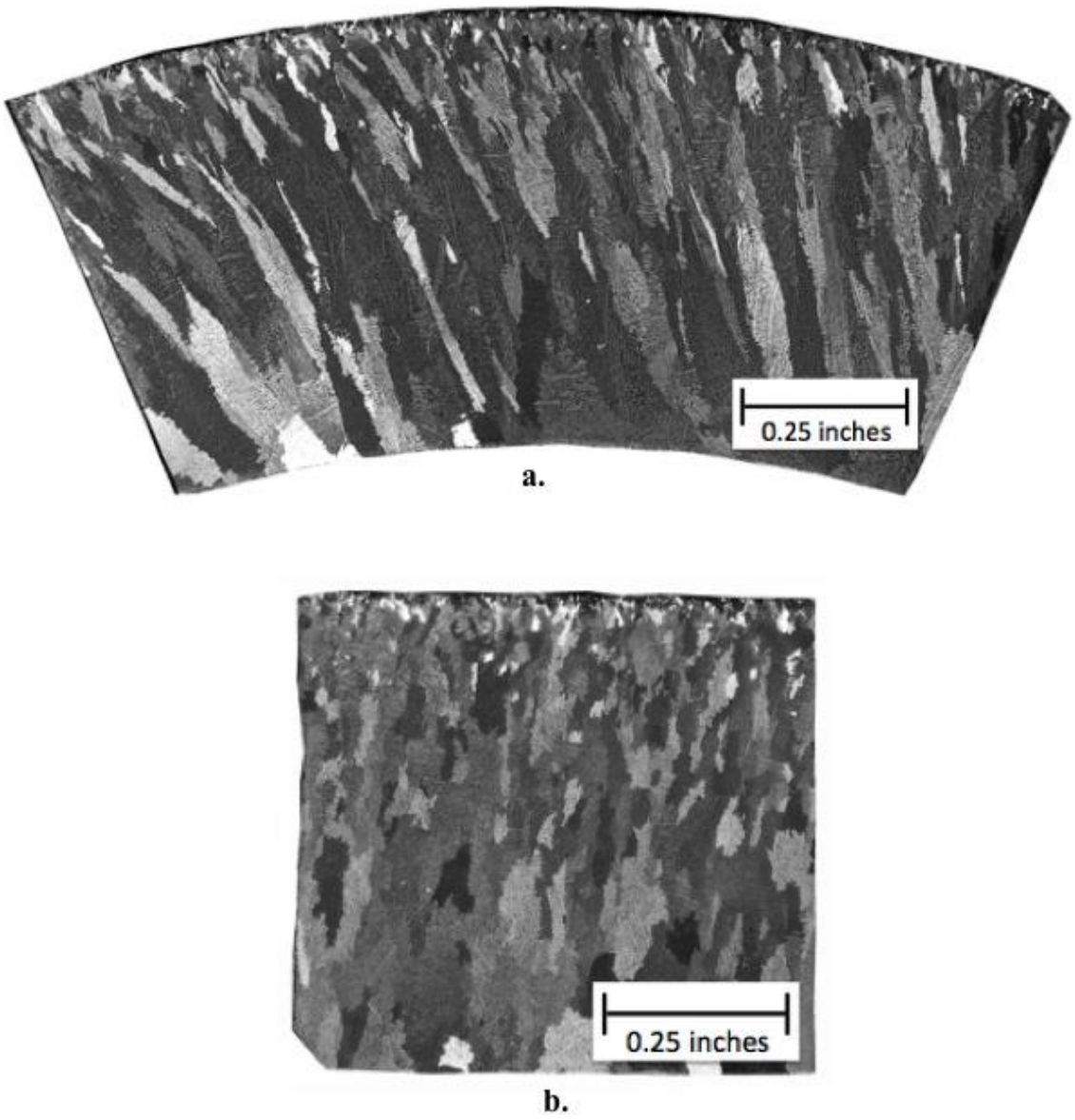

Figure 29. Transverse (a) and longitudinal (b) photo macrographs of service exposed HP alloy tube sample 7M3P4.

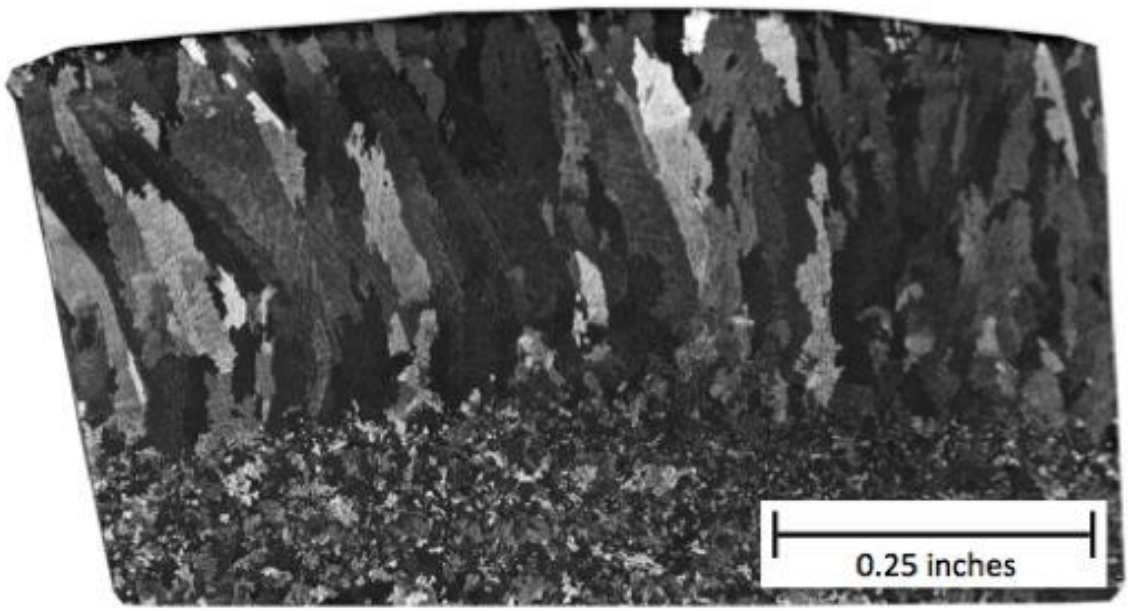

a.

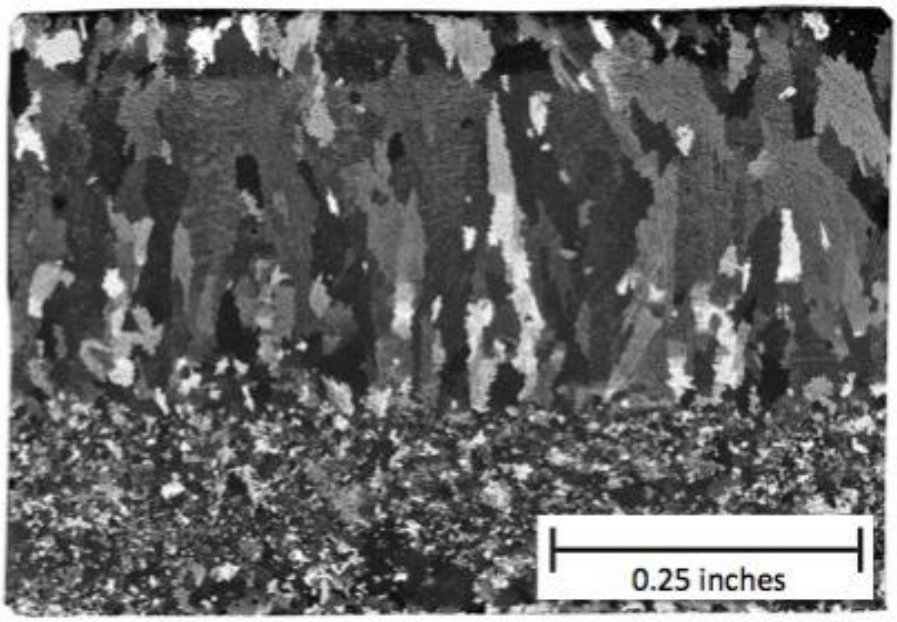

b.

Figure 30. Transverse (a) and longitudinal (b) photo macrographs of service exposed HP alloy tube sample 8M3P5.

6.5.2: Percent Fine Grain Evaluation

The measured percentages of fine grains in the provided HP alloy tube samples are reported in Table 9. As is shown, the amount of fine grains in the tube walls varies greatly even between tubes from the same manufacturer. This variability in fine grain formation is predominantly due to the dynamic nature of the centrifugal casting process, with the formation of columnar and equiaxed fine grains controlled by the speed of rotation of and the amount of vibration in the cylindrical mold. Inadvertent speeding up or slowing down the rotational speed of the mold from the speed optimized for columnar grain formation causes turbulence in the molten metal and the formation of fine equiaxed grains at unexpected locations in the wall of the tube. In addition, excessive vibration of the mold can have the same turbulent effect as changing the rotational speed.

Table 8. Percent fine grain analysis results taken from macro etched samples of the service exposed HP alloy tube samples.

Sample:	Percent Fine Grains in Tube Wall:	Location:
1M1P1	All Columnar	N/A
2M1P1	45	Inside Diameter
3M2P2	90	Inside Diameter
4M3P3	Extreme Variability	N/A
5M3P3	15	Inside Diameter
6M3P4	35	Inside Diameter
7M3P4	5	Outside Diameter
8M3P5	35	Inside Diameter

7: Conclusions

The tube samples from manufacturer M1 experienced less service damage than the tubes from manufacturers M2 or M3. Of the eight different heats, the samples from manufacturer M1 showed a higher carbon content and a lower level of alloying elements in comparison to the other tubing heats. In addition, the M1 tubes had the greatest extent of precipitated secondary carbides and in general they had the lowest volume percent of voids. Taking into consideration the reported information on each of the tubes, it must also be noted that the M1 tubes had also experienced the highest operating temperatures and spent the longest amount of time in service. As is mentioned in the general information provided in Table 1, no ruptures or indications of damage were noticed in the M1 tubes during service. The tube from manufacturer M2 was removed from service because eddy current inspection detected damage in the wall of the tube. One of the five tubes from manufacturer M3 ruptured during service. Two additional M3 tubes were removed from service because of proximity to or exhibiting similar behavior as a ruptured tube at the same facility.

After reviewing the information above it can be concluded that void growth preferentially occurs in the fine grain regions of the HP alloy tubes, with the greatest amount occurring within the last five percent of the sample's life. This makes it difficult to determine when a tube is about to rupture, as there is only a narrow window of time in which the damage can be detected before rupture.

More exact conclusions concerning tube durability could not be reached due to the variability among the samples. As is shown in Section 6.5, the tube macrostructures exhibited extreme variability in the relative proportions of columnar grains and equiaxed grains. This variability not only exists between the three tube manufacturers, but between the tubes from the same manufacturer. Another source of error was the fact that the ex-service tubes came from a total of five different plants, resulting in a wide variety of time and temperature exposures. In addition, the tubes were not all removed from comparative locations at the five different plants. This variability in location is compounded due to the fact that the ring samples from the ex-service tubes were removed from different sections of the sample tubes rather than being removed from the same location to aid in comparison. Furthermore, the location on the ex-service tubes where

the creep test samples were removed is unknown. This makes it difficult to compare the ex-service ring samples to the creep test samples from the ex-service tubes.

The greatest obstacle encountered in this project was the variability of the calculated volume percentage of voids within the tube walls. During evaluation of the images used for the volume percent void assessment, it was found that the point-counted void area can differ up to fifty percent or more between images obtained as little as five hundredths of an inch apart. Taking this observation into account, the reason for the apparent decrease in the calculated volume percent of voids that some of the samples experienced after creep testing can be understood. Since the creep test samples were removed from different sections of the tube than were the ring sections and the calculated volume percent of voids was found to deviate so much between adjacent images, it is not unexpected for the calculated volume percent values to deviate from the expected trend that the amount of voids in the material will increase under applied creep stress (since the service exposed and creep tested samples were removed from different sections of the same parent tube). This type of error is usually minimized in industry by removing a series of ring sections along the length of the tube in order to create an average that better represents the true condition of the inspected tube than measurements performed on a single ring sample.

References

[1] Buchanan, Karl G. “The Effects of Long-Term Isothermal Ageing on the Microstructure of HP-Nb and HP-NbTi Alloys.” The University of Canterbury, Christchurch, New Zealand. 2013.
[2] Matesa, B.; Samardzic, I.; Bodenberger, B; Sachs, B.P.; and Pecic, V. “Eddy Current Inspection in Processing Furnace Remaining Life Prediction.” Proceedings of the IIW International Conference Safety and Reliability of Welded Components in the Energy and Processing Industry. 2008. P. 359-364.
[3] Schillmoller, C.M. “HP-Modified Furnace Tubes for Steam Reformers and Steam Crackers.” Nickel Development Institute. NiDi Technical Series, No. 10058. Mar. 1991.
[4] ASTM Standard A297, 2010. “Standard Specification for Steel Castings, Iron-Chromium-Nickel Heat Resistant, for General Application.” ASTM International, West Conshohocken, Pa. 2010. DOI: 10.1520/A0297_A0297M-10. <http://www.astm.org>.
[5] ASTM Standard A608, 2012. “Standard Specification for Centrifugally Cast Iron-Chromium-Nickel High-Alloy Tubing for Pressure Application at High Temperatures.” ASTM International, West Conshohocken, Pa. 2012. DOI: 10.1520/A0608_A0608M-12. <http://www.astm.org>.
[6] “Castings- Stainless Steel and Nickel-Base.” Nickel Institute. < http://www.nickelinstitute.org/en/TechnicalLiterature/Reference% 20Book%20Series/11022_CastingsStainlessSteelandNickelBase.aspx >. May 9, 2013.
[7] Lundin, C.D.; Liu, W.; Zhou, G.; and Liu, P. “Microstructural Evaluation of Modified & Microalloyed HP Alloys in As-cast & Creep Tested Conditions.” Materials Joining Research, Materials Science and Engineering, The University of Tennessee, Knoxville, TN. 2000.
[8] “Cast Heat-Resistant Alloys.” The International Nickel Company, Inc. 1974. < http:// www.nickelinstitute.org/~/Media/Files/TechnicalLiterature/CastHeat_Resistant Alloys_1196_.pdf >.
[9] da Silveira, Tito L. and May, Ian L. “Reformer Furnaces: Materials, Damage Mechanisms, and Assessment.” The Arabian Journal for Science and Engineering. Vol. 31, No. 2C. Dec. 2006. P. 99-119.

[10] Ruud, C.O.; Diaz, A.A.; Anderson, M.T. “Grain Structure Identification and Casting Parameters of Austenitic Stainless Steel (CASS) Piping.” U.S. Department of Energy, Pacific Northwest Laboratory. Nov. 2009.
[11] Joshi, Amit M. “Centrifugal Casting.” Department of Metallurgical Engineering & Materials Science, Indian Institute of Technology. Bombay, India.
[12] Madhusudhan, Narendranath S.; Kumar, G.C. Mohan. “Experimental Study on Cooling Rate of Centrifugal Casting Based on Grain Size.” International Journal of Scientific Engineering Research. Vol. 13, Issue 1. January 2012.
[13] Barbabela, Gloria Dulce; de Almeida, Luiz Henrique; da Silveira, Titl Luiz; May, Ian Le. “Phase Characterization in Two Centrifugally Cast HK Stainless Steel Tubes.” Materials Characterization 26, Elsevier Science Publishing. 1991. P. 1-7.
[14] May, I.L.; da Silveira, T.L.; Vianna, C.H. “Criteria for the Evaluation of Damage and Remaining Life in Reformer Furnace Tubes.” International Journal of Pressure Vessels and Piping. Vol. 6, Issues 1-3. 1996. P. 233-241.
[15] Wen-Tai, Hou; Honeycombe, R.W.K. “Structure of Centrifugally Cast Austenitic Stainless Steels: Part 1 HK 40 as Cast and After Creep Between 750 and 1000°C and Part 2 Effects of Nb, Ti, and Zr.” Materials Science and Technology. Vol. 1. May 1985. P. 385-397.
[16] Swaminathan, Jaganathan; Guguloth, Krishna; Gunjan, Manojkumar; Roy, Prabirkumar; Ghosh, Rabindranath. “Failure Analysis and Remaining Life Assessment of Service Exposed Primary Reformer Heater Tubes.” Materials Science and Technology Division, National Metallurgical Laboratory, Jamshedpur, Jharkhand, India. Mar. 2, 2007.
[17] Shannon, Brian and Jaske, Carl. “A Comprehensive Approach to Reformer Inspection and Assessment.” Second Middle East Nondestructive Testing Conference and Exhibition. Dec. 8-10, 2003.
[18] May, I.L.; da Silveira, T.L.; Cheung-Mak, K.P. “Uncertainties in the Evaluation of High Temperature Damage in Power Stations and Petrochemical Plants.” International Journal of Pressure Vessels & Piping 59, Elsevier Science Publishing. 1994. P. 335-343.

[19] da Silveria, T.L. and Le May, I. “Effects of Metallographic Preparation Procedures on Creep Damage Assessment.” Materials Characterization. Vol. 28, Issue 1. Jan. 1992. P. 75-85.
[20] ASTM Standard E562, 2011. “Standard Test Method for Determining Volume Fraction by Systematic Manual Point Count.” ASTM International, West Conshocken, PA. 2011. DOI: 10.1520/E0562-11. < http://www.astm.org >.

Vita

Zane Palmer is the eldest of three children born to parents Randy and Jackie Palmer. Having been born in Knoxville, TN, he was raised in Maryville, TN where he graduated with honors from Maryville High School in May of 2008. After high school, he attended the University of Tennessee, Knoxville where he earned a Bachelors of Science in Materials Science and Engineering in May of 2012. In August of 2012, Zane re-entered UT as a Graduate student in the Materials Science and Engineering Department where he worked as both a Graduate Research Assistant and a Graduate Teaching Assistant. Zane graduated with a Masters of Science degree in Materials Science and Engineering in August of 2014.